Novel insights in the pathophysiology of α-synuclein dysregulation on D2 receptor activity contributing to the vulnerability of dopamine neurons

Abeer Dagra[1#], Douglas R. Miller[1#], Fatemeh Shaerzadeh[1], Min Lin[1], Adithya Gopinath[1], Sharonda Harris[1], Zachary A. Sorrentino[1], Sophia Velasco[1], Adetola R Alonge[1], Janelle Azar[1], Joe J Lebowitz[1], Brittany Ulm[1], Anthea-Mengfei Bu[1], Carissa A. Hansen[1], Nikhil Urs[1], Benoit I. Giasson[1*], Habibeh Khoshbouei[1*]

[1] Department of Neuroscience, University of Florida; Gainesville, Florida, USA.

#These authors contributed equally to this work.
*Corresponding Authors:
habibeh@ufl.edu
bgiasson@ufl.edu

Abstract

Pathophysiological damages and loss of function of dopamine neurons precedes their demise and contributes to the early phases of Parkinson's disease. The presence of aberrant intercellular pathological inclusions of the protein α-synuclein within ventral midbrain dopaminergic neurons is one of the cardinal features of Parkinson's disease. We employed multiple complementary approaches in molecular biology, electrophysiology, and live-cell imaging to investigate how excessive α-synuclein levels alters multiple characteristics of dopaminergic neuronal dynamics and dopamine transmission prior to neuronal demise. These studies demonstrate that α-synuclein dysregulation of D2 receptor autoinhibition contributes to the vulnerability of dopaminergic neurons, and that modulation thereof can ameliorate the resulting pathophysiology. These novel findings provide mechanistic insights in the insidious loss of dopaminergic function and neurons that characterize Parkinson's disease progression with significant therapeutic implications.

Introduction

Volitional movement is a crucial fundamental behavior of everyday life that is often taken for granted until control diminishes and deteriorates. Dopaminergic neurons within the ventral midbrain play a critical role in the initiation and control of volitional movement[1,2] and the progressive demise of these neurons is a defining hallmark of Parkinson's disease (PD)[3]. Pathophysiological damages and loss of function of these neurons precedes their demise and contributes to the early phases of the movement impairments[4]. No current therapies reverse or ameliorate the insidious nature of PD or the many related neurodegenerative diseases associated with the demise of dopaminergic neurons. The lack of a better understanding of the etiology of PD greatly impedes the ability to identify therapeutic targets to slow this detrimental progression.

The presence of aberrant intercellular, pathological inclusions comprised of the protein α-synuclein (α-syn) in the form of Lewy bodies and Lewy neurites within ventral midbrain dopaminergic neurons is another cardinal feature of PD [5–7]. Several missense mutations in the α-syn gene (*SNCA*) can be responsible for familial PD, but the duplication[8] or triplication[9] of *SNCA* are also sufficient to cause PD and the related disease Lewy body dementia. Thus, only a 50% increase in the expression of wild type α-syn as in the duplication of the *SNCA* gene is sufficient for detrimental outcome on dopaminergic neurons resulting in disease. Furthermore, some studies indicate that elevated α-syn levels also occurs in idiopathic PD, but the pathophysiological mechanisms associated with increased levels of α-syn remain poorly understood.

In the studies, herein, extensive complementary approaches in molecular biology, electrophysiology, and live-cell imaging were utilized to investigate the effects and outcomes of α-syn elevated expression on dopaminergic neuronal dynamics, intraneuronal calcium homeostasis and dopamine transmission prior to neuronal demise. It is demonstrated that D2 receptor autoinhibition, contributes to alterations in neuronal homeostatic properties, and that modulation thereof can ameliorate the pathophysiology resulting from excessive α-syn levels. These results provide novel mechanistic insights in the pathobiological impact of α-syn on dopaminergic neuron function and their demise characteristic of the insidious nature of PD.

Results and discussion

Tyrosine hydroxylase promoter-driven adeno-associated virus (AAV) efficiently transduces and express human α-synuclein in cultures midbrain dopamine neurons. In order to investigate the pathophysiology changes associated with α-syn overexpression we first develop a cell model with high fidelity expression of human α-syn in midbrain dopaminergic neurons. We utilized a tyrosine hydroxylase (TH) promoter-driven adeno-associated virus (AAV) to specifically express wild-type human α-syn in these cultured dopaminergic neurons. First to demonstrate the specificity of this vector, cultures were transduced with the virus expressing GFP. As demonstrated in Figure 1A-B, 91% ± 3 of neurons expressing GFP- are TH-positive, indicating high specificity. The same pAAV1-TH backbone but with the human α-syn cDNA, was utilized to overexpress human α-syn in dopamine neurons. The transduction of pAAV1-TH-human-αsyn in

cultured midbrain dopamine neurons was confirmed via immunocytochemistry and western blot analyses, demonstrating elevated expression of α-syn these neurons (Figure 1C-D, Supplemental Figure 1, p = 0.005, two-tailed t-test, n = 3 independent experiments).

Overexpression of α-synuclein disrupts calcium dynamics and firing activity of dopamine neurons. Increased α-syn burden in dopamine neurons is correlated with neuronal loss in neurodegenerative diseases such as Parkinson's disease (PD)[10,11]. Although extensively studied in cortical neurons, yeast, and heterologous expression systems [12–17], α-syn regulation of intracellular calcium and firing activity in dopaminergic neurons prior to cell death remains less clear. Maintenance of calcium homeostasis is a vital process in neurons[18–20]. Calcium is a ubiquitous second messenger that helps to transmit depolarization status and synaptic activity to the biochemical machinery of a neuron[21]. High intensity calcium signaling requires high ATP consumption to restore basal (low) intracellular calcium levels. Increased intracellular calcium may also lead to increased generation of mitochondrial reactive oxygen species[22,23]. Impaired abilities of neurons to maintain cellular energy levels and to suppress oxygen species may impact calcium signaling during aging and in neurodegenerative disease processes[5,6]. To investigate if α-syn overexpression regulates dopaminergic neuronal activity prior to neuronal demise, we employed live cell calcium imaging recording in DAT-Cre-GCaMP6f-expressing dopamine neurons containing either endogenous levels of α-syn (naive) or overexpressing α-syn. Compared to the modest calcium events in naive dopaminergic neurons, both width and amplitude were increased in the presence of α-syn overexpression, creating repeated burdens on the neuron (Figure 2A-C, width - $p = 0.034$, one-way ANOVA, $F(2,97) = 3.89$, n = 33 wild type neurons, n = 40 α-syn overexpressing neurons, amplitude - $p = 0.000002$, one-way ANOVA, $F(2,1294)=12.62$, n = 33 wild type neurons, n = 40 α-syn overexpressing neurons). These data suggest that increased levels of α-syn in dopamine neurons leads to disturbances in calcium homeostasis that can alter biophysical properties of neurons, neuronal activity, neurotransmission[20,24–29] and neuronal death, all of which are shared hallmarks in neurodegenerative diseases[24,30–32].

While measurement of calcium activity provides inferential information about neuronal firing, we did not observe a change in calcium event rates (Figure 2C, left). To directly test whether α-syn overexpression modulates firing activity of dopaminergic neurons, we utilized whole-cell current clamp recordings to measure the spontaneous firing activity of these neurons. While dopaminergic neurons containing an endogenous level of α-syn exhibited the characteristic pacemaker-like firing activity[33,34], the spontaneous firing activity of α-syn overexpressing dopamine neurons showed an irregular and clustered firing pattern with increased burst firing activity within the clusters (Figure 2 D-E, from eight independent experiments, 1.132 ± SEM for naive neurons vs. 3.187 ± SEM for α-syn overexpressing neurons, one-way ANOVA, followed by Tukey's HSD, $F(2,20) = 6.092$, WT vs α-syn $p = 0.0123$). Thus far, our data suggest that increased α-syn levels in dopaminergic neurons lead to altered calcium dynamics and increased firing activity. Both firing activity and calcium dynamics in dopamine neurons are tightly regulated by the activity of the D2 autoinhibitory receptors[33–37]. Therefore, we asked whether α-syn-

induced dysregulation of dopamine neuronal activity and calcium dynamic are due to reduced D2-receptor autoinhibition.

α-synuclein overexpression reduces D2-receptor autoinhibition. Multiple channels and transporters regulate neuronal activity and intracellular calcium dynamics. Dopamine activation of D2 autoinhibitory receptors on dopamine neurons decreases neuronal activity[33–36,38,39] and intracellular calcium dynamics[31,35,40–43]. Therefore, we tested the hypothesis that the observed disturbance in neuronal excitability and calcium dynamics in α-syn overexpressing neurons is due to dysregulation of canonical D2 receptor (D2R) autoinhibition in these neurons. In a double-blinded experimental design, we exposed DAT-Cre-GCaMP6f-expressing dopaminergic neurons to dopamine (1 μM) while monitoring the change in GCaMP6f signal. Consistent with the literature[44,45], naive neurons exhibited the characteristic decreased fluorescence during exposure to extracellular dopamine intensity (Figure 3A,B – top, n = 14-21, two-way ANOVA where the variables are time and treatment, followed by Tukey's HSD, p = 0.0003, from five independent replicates). However, α-syn overexpressing neurons exhibited attenuation to dopamine-induced reduction of GCaMP6f signal, (n = 17-26, two-way ANOVA where the variables are time and treatment, followed by Tukey's HSD, p = 0.0088, from five independent replicates). Further, fold change responses of naive dopamine neurons were significantly stronger than α-syn overexpressing neurons (Figure 3C, n = 11-17, one-way ANOVA followed by Tukey's HSD, WT vs. α-syn, p = 0.0035, WT vs. GFP p = 0.2927 and α-syn vs. GFP p = 0.0001, from five independent replicates, Supplemental Figure 2A). These data suggest α-syn overexpression decreases inhibitory feedback regulation of dopamine neurons of intraneuronal calcium activity.

While these data support the interpretation that α-syn overexpression decreases the feedback modulation of neuronal activity, they do not unequivocally show a decrease in D2 receptor activity. Dopamine interacts with multiple targets, such as dopamine transporter that also regulate neuronal excitability[46–49] and intracellular calcium activity[46,48,50–52]. Therefore, we utilized quinpirole, a D2R-specific agonist, (10 μM) to stimulate D2R in DAT-Cre-GCaMP6f-expressing dopamine neurons containing either endogenous levels of α-syn or its overexpression (Figure 3D). Consistent with the literature [41,43,44,53], quinpirole activation of D2 autoinhibitory receptors induced the canonical suppression of calcium dynamic in dopaminergic neurons, whereas calcium activity in α-syn overexpressing neurons did not change calcium dynamic during quinpirole administration (Figure 3E,F naive : n = 11-21, two-way ANOVA where the variables are time and treatment, p = 0.0007, from five independent replicates; α-syn: n = 13-26, two-way ANOVA where the variables are time and treatment, p = 0.7259, from five independent replicates, fold change comparisons – n = 11-13, one-way ANOVA followed by Tukey's HSD, naive vs. α-syn, p = 0.0318, naive vs. GFP p = 0.8178, and α-syn vs. GFP p = 0.0057, from five independent replicates, Supplemental Figure 2B).

Although live cell calcium imaging provides a proxy for dopamine neuronal activity[50], calcium imaging does not reveal changes in firing activity at the resolution of electrophysiological recordings. Therefore, as a complementary approach, we utilized whole-cell current clamp recordings to compare the spontaneous firing activity of naive

and α-syn overexpressing dopaminergic neurons following quinpirole administration. Consistent with the literature, quinpirole activation of D2 autoreceptors decreased the firing activity of WT dopamine neurons[36,38,54–56]. Whereas, the response to quinpirole in α-syn overexpressing neurons is significantly attenuated (Figure 3G-J, n = 7 from independent experiments, 0.1812 ± SEM for naive neurons vs. 0.7930 ± SEM for α-syn treated with quinpirole, two-tailed unpaired t-test, p = 0.0356, interspike interval – n = 7 from independent experiments, 11,118 ± SEM for naive neurons vs. 3786 ± SEM for α-syn neurons treated with quinpirole, two-tailed unpaired t-test, p = 0.1197, firing regularity (CV of ISI) – n = 7 from independent experiments, 2.06 ± SEM for WT neurons vs. 1.659 ± SEM for α-syn neurons treated with quinpirole, two-tailed t-test, p = 0.4507). Surprisingly, we observed that the longer the exposure to quinpirole, the firing activity of α-syn overexpressing dopamine neurons began to resemble naive dopaminergic neurons at baseline (before drug application, end of quinpirole treatment of α-syn neuron recording, Figure 3G – right, pink). Collectively, these data support the idea that α-syn overexpression reduces the efficacy of D2 receptor autoinhibition in dopamine neurons and a prolonged activation of D2 receptor can potentially restore this deficit.

α-synuclein overexpression increases intra- and extracellular dopamine levels and tyrosine hydroxylase expression. Our findings so far suggest that α-syn may induce a feed-forward adaptive mechanism that decreases the ability of inhibitory D2 autoreceptors to act as a break on neuronal excitability and increasing extracellular dopamine levels[33,36]. To test this hypothesis, we used two complementary approaches to measure intra- and extracellular dopamine levels. First, we used $GRAB_{DA4.4}$ (G protein-coupled receptor [GPCR]-activation-based DA) sensor-expressing HEK293 cells to measure extracellular dopamine levels. $GRAB_{DA4.4}$ is a genetically encoded fluorescent dopamine sensor, engineered by coupling a conformationally-sensitive circular-permutated EGFP (cpEGFP) to D2 receptor. In $GRAB_{DA4.4}$-expressing HEK293 cells, dopamine binding to the sensor induces a conformational change which results in a robust increase in fluorescence signal in a concentration-dependent manner (Figure 4A-B). Constitutive $GRAB_{DA4.4}$ fluorescence signal in the absence of dopamine neurons (in the culture) was obtained at the beginning of each experiment, where the cells were plated in similar conditions sans neurons (F_c, Figure 4C). To compare baseline dopamine release amongst the experimental groups, the average ratio of fluorescence signal of cells adjacent to the soma and neuronal processes to the average ratio of fluorescence signal of $GRAB_{DA4.4}$ cells (only) were calculated ($F_{baseline} = (F_{GRABDA4.4\ cells\ grown\ with\ neurons} - F_c) / F_c$). To compare KCl stimulation of dopamine release, the changes on the average fluorescence signal of cells adjacent to the soma and neuronal processes before and after KCl were calculated ($\Delta F/F = (F_{stimulated} - F_{baseline}) / F_{baseline}$). Co-culture of $GRAB_{DA4.4}$ cells with dopamine neurons 20-24 hours prior to live cell confocal imaging enabled real-time detection of endogenous dopamine released from the neurons at baseline, i.e. spontaneous dopamine release (Figure 4D, E). Using a double-blinded experimental design, we found a significantly higher basal extracellular dopamine level, as measured by a higher $GRAB_{DA4.4}$ fluorescence signal around the soma and neuronal processes of α-syn overexpressing neurons (Figure 4F, n = 10 from three independent replicates; the data are means ± SEM, one-way ANOVA followed by Tukey's HSD, F(2,167) = 13.05, naive vs. α-syn p = 0.0007, WT vs. GFP p = 0.9866 and GFP vs. α-syn p = 0.0001). These

data support the interpretation that α-syn-induced stimulation of spontaneous neuronal activity leads to increased extracellular dopamine levels. As a positive control group, we measured the $GRAB_{DA4.4}$ fluorescent signal around the soma and neuronal processes following KCl (90mM) stimulation of dopamine release [57]. KCl-induced neuronal depolarization [58,59] produced a robust fluorescence increase that was not different amongst the experimental groups (Figure 4G, n = 10 from three independent replicates; the data are mean ± SEM analyzed by one-way ANOVA followed by Tukey's HSD, $F(2,68) = 0.2540$, naive vs. α-syn $p = 0.9872$, naive vs. GFP $p = 0.8651$ and GFP vs. α-syn $p = 0.7827$). Consistent with our previous report, these data suggest that α-syn overexpression decreases dopamine uptake via the dopamine transporter (DAT) [60] and increases the DAT-mediated dopamine efflux [61] leading to increased extracellular dopamine levels. Collectively, these data provide a reasonable cellular mechanism for the puzzling observation by Lam et al., that in mice overexpressing α-syn there is an initial increase in extracellular dopamine levels in the striatum prior to neuronal death [62].

As a complementary approach, via a double-blinded experimental design, we used HPLC to measure dopamine level in the external milieu of naive dopaminergic neurons and dopaminergic neurons overexpressing α-syn. HPLC analysis (see Methods) showed a significantly higher extracellular dopamine in α-syn overexpressing neurons compared to naive neurons or dopaminergic neurons expressing GFP (Figure 4H, I; n = 8 each, from 8 independent replicates; one-way ANOVA followed by Tukey's HSD, $F(3,22) = 9.525$, WT vs. α-syn $p = 0.01$, WT vs. GFP $p = 0.5235$ and GFP vs. α-syn $p = 0.0005$). Collectively, these data, combined with live cell detection of extracellular dopamine levels, support the notion that α-syn modulation of dopaminergic neuronal activity leads to increased extracellular dopamine that could be due to increased neuronal activity, increased dopamine synthesis, or both possibilities. Since we have already examined the former (Figure 4F,H), to test the latter possibility, we used HPLC to measure intracellular dopamine levels via a double-blinded experimental design (described in Methods). The measurement of dopamine in the cell lysate of naive and α-syn overexpressing neurons revealed a significantly higher intracellular dopamine (Figure 4 I, n = 8 each, from 8 independent replicates, one-way ANOVA followed by Tukey's HSD, $F(3,22) = 9.376$, naive vs. α-syn $p = 0.0059$, naïve vs. GFP $p = 0.5164$ and GFP vs. α-syn $p = 0.0003$). These data suggest that the decreased autoinhibition of dopamine neurons following α-syn overexpression not only increases neuronal excitability, but also dysregulates dopamine synthesis and secretion. Furthermore, in Figure 2, we showed that increased neuronal α-syn increases the magnitude and duration of intracellular calcium burden, which would promote increased basal dopamine release.

Multiple mechanisms likely contribute to the increased intracellular dopamine following α-syn overexpression. For example, increased dopamine uptake via the dopamine transporter (DAT), decreased DAT-mediated dopamine efflux, increased expression of tyrosine hydroxylase (TH), a key enzyme involved in dopamine synthesis, or a combination of these mechanisms would possibly contribute to a higher intracellular dopamine level. Previously, we and others have shown that α-syn overexpression reduces dopamine recycling by reducing dopamine uptake [60,63,64]. In addition we have shown that α-syn overexpression, increases reverse transport of dopamine i.e. dopamine

efflux [61], without changing surface DAT levels. Therefore, α-syn regulation of dopamine uptake or dopamine efflux would decrease intracellular dopamine, not increase it.

Whereas α-syn regulation of DAT activity predicts a decrease of intracellular dopamine level[60,61,63–65], D2 receptor activity negatively regulates TH protein levels as a compensatory mechanism to down-regulate dopamine synthesis [36,43,66–69]. As shown in Figure 2 and Figure 3, we found a reduction in the canonical D2 receptor autoinhibition of dopamine neurons, likely modulating downstream signaling cascades that can regulate TH protein levels. Therefore, next we tested the hypothesis that increased TH levels caused by reduced D2 autoinhibition in α-syn overexpressing neurons (as observed in Figures 2, 3) underlies the increased intracellular dopamine[66,69–74]. Since the frequently used approaches of western blotting or immunocytochemistry do not provide purely quantitative data of protein expression to test this hypothesis, we developed an ELISA to quantify TH levels in α-syn overexpressing neurons (Figure 4 J). For these experiments we used HEK293 cells as a negative control group and PC12 cells as a positive control group (Figure 4 L). Purified full-length recombinant TH protein was used to generate a standard curve (Fig 4 K). α-syn overexpressing neurons show significantly higher TH levels, compared to naive and control conditions (Figure 4M, n = 8-10, one-way ANOVA followed by Tukey's HSD, $F(2,23) = 4.488$, naive vs. α-syn $p = 0.031$, naive vs. GFP $p = 0.7983$, and GFP vs. α-syn $p = 0.0491$). While ELISA provides quantitative data for total TH level across these experimental groups, a limitation of this assay is that it cannot discriminate TH phosphorylation that is associated with TH activity and thus dopamine synthesis[66,75,76]. Nevertheless, these data support the interpretation that increased intracellular dopamine in α-syn overexpressing neurons, at least in part, is due to increased TH protein levels.

Altered neural dynamics mediated by α-synuclein may emerge from altered D2 activity and expression patterns. Our data, so far, support the interpretation that the canonical D2 receptor autoinhibitions, such as inhibitory modulation of spontaneous firing activity, is reduced in α-syn overexpressing neurons. While D2 receptor agonist quinpirole silenced naive dopamine neurons, the response to quinpirole in α-syn overexpressing neurons is significantly delayed and reduced, possibly due to desensitization or reduced activity of the D2 receptor (Figure 3). Therefore, next we tested the hypothesis that blockade of D2 receptor in naive dopaminergic neurons simulates the firing activity observed in α-syn overexpressing neurons. We performed whole-cell current clamp recordings to measure spontaneous firing activity of dopaminergic neurons before and during bath application of sulpiride (D2 antagonist, 5 μM). In naive dopaminergic neurons, bath application of sulpiride produced burst firing patterns with intermediated periods of quiescence and firing frequencies resonant with neuronal activity seen in α-syn overexpressing dopaminergic neurons (Fig 5 A-E, n = 8 from 3 independent biological replicates, two-tailed unpaired t-test, firing frequency: 1.766 ± SEM naive vs. 2.805 ± SEM α-syn overexpressing neurons, $p = 0.148$, ISI – 1791 ± SEM naive vs. 1221 ± SEM α-syn overexpressing neurons $p = 0.1147$, CV of ISI - 1.642 naive ± SEM vs. 1.412 ± SEM α-syn overexpressing neurons, $p = 0.456$). These data support the hypothesis that in α-syn overexpressing dopamine neurons, the reduced functional availability of D2-mediated

response could be due to receptor desensitization [77,78], decreased membrane expression of D2 receptors, or a combination of these possibilities.

To investigate if α-syn overexpression in dopaminergic neurons alters D2 receptor expression, we performed cell surface biotinylation of D2 receptor via a double-blinded experimental design. We found increased ratio of average cytoplasmic D2R to average total D2R in α-syn overexpressing neurons (Figure 5 F, n = 3 from independent replicates, two-tailed unpaired t-test, p = 0.1115). Whereas the ratio of average membrane D2R to the average cytoplasmic D2R decreased compared to naïve neurons (Figure 5 G, from 3 independent replicates, two-tailed unpaired t-test, p = 0.0178). The double immunocytochemistry of fixed but not permeabilized dopamine neurons stained for both D2R and an integral membrane protein such as Na+/K+-ATPase, or GM1-CTxB would have been a suitable complementary approach to examine membrane localized D2R across the experimental groups in this study. However, the frequently used D2R antibodies in the field[77–80] are raised against the intracellular N-terminal domain of the receptor. This limitation decreases the confidence in identification of membrane vs. intracellular protein levels. Similar technical limitation applies to the single cell qPCR assay, where total transcript levels do not necessarily reflect functional D2Rs at the membrane. The latter limitation somewhat applies to the biotinylation assay used in this study. Unless an antibody is raised against the active or inactive form of the receptor, a biotinylation assay detects both functional and desensitized receptors. Therefore, although our data suggest membrane D2Rs are decreased in α-syn overexpressing neurons, it is possible that the detected membrane D2Rs are desensitized, i.e. a lesser receptor-effector coupling[81–84]. Therefore, live cell functional assays, such as electrophysiology and calcium imaging, combined with pharmacological manipulations are more reliable strategies to assess the mechanism of α-syn regulation of neuronal activity.

α-synuclein overexpression reduces arborization of dopamine neurons and pretreatment with a D2 receptor agonist partially rescues the detrimental impact of α-synuclein. Dopaminergic neurons have extensive axonal arborizations and large terminal fields [85–87], where one dopamine neuron is estimated to have ~245,000 release sites[88,89]. Studies in animal models of PD and postmortem data in human PD[90] show decreased axonal complexity and dendritic arborization, reduction of number of axon terminals and global neuronal size precede neuronal death[63,88,91]. Our data suggest that prior to cell death, via a D2 receptor mechanism, α-syn overexpression can induce neuronal disinhibition, leading to increased intra- and extracellular dopamine levels that are implicated in increased neuronal vulnerability[13,92,93]. Therefore, we investigated the potential link between α-syn-mediated dopamine neuronal dysfunction and neuronal complexity.

Sholl analysis entails using concentric circles around the soma of a neuron, with dendritic fields intersecting these concentric circles counted as a measure of differences in neuronal complexity (Figure 6 A-D). This analytical approach estimates[87,94–96] neuronal complexity via assessment of projection area, number of intersections as a measure of neuronal arborization, projection field perimeter, neuronal arborization width, and circularity of dendritic arborization[94,96–100]. Compared to naive dopaminergic neurons, α-

syn overexpressing neurons exhibit a lower degree of neuronal arborization (Figure 6 E, F, H), reduced projection arborization area (Fig. 6 J), reduced circularity of dendritic arborization (Fig 6 K), smaller dendritic projection perimeter (Fig. 6 L), and smaller arborization width (Fig. 6 M), but no change in the soma area (Fig 6 I, one-way ANOVA followed by Tukey's test, naive n = 190, α-syn n = 114, intersections: naive vs. α-syn p = 0.0009, circularity: naive vs. α-syn p = 0.0021, outer perimeter: naive vs. α-syn p = 0.0001; width: WT vs. α-syn p = 0.0001, projection area: naive vs. α-syn p = 0.0001, soma area: naive vs. α-syn p = 0.67, from at least three independent biological replicates). The loss of neuronal complexity and decreased dendritic arborization found in this study are consistent with morphological data in postmortem PD samples[90], potentially informing the progression of α-syn-induced pathology prior to neuronal loss.

The unexpected observation, that prolonged bath application of D2 receptor agonist began to restore the firing properties of α-syn overexpressing neurons to the levels measured in WT dopamine neurons at baseline (end of quinpirole treatment of α-syn neuron recording, Figure 3G – right, pink), suggests that pharmacological activation of D2 receptor is a potential target to alleviate α-syn pathology prior to neuronal death. This hypothesis is consistent with reports showing that D2 receptor activation sustains structural plasticity of dopaminergic neurons by maintaining their dendritic arborization [93,101–104]. Therefore, we tested whether the “retrograde axonal degeneration” hypothesis described in the literature[105,106] could be ameliorated through D2 receptor activation, leading to restoration or reduction of the declining degree of neuronal complexity[93,107,108]. We measured neuronal complexity when α-syn overexpressing neurons were pretreated with quinpirole (0.5 μM) for 48-hours. Surprisingly, we found that quinpirole produced a marked improvement in dendritic arborization of α-syn overexpressing neurons (Figure 6D, G). Detailed morphometrical analysis revealed no change in somatic size of neurons across all experimental groups; whereas, quinpirole restored neuronal circularity, perimeter of the projection field, projection perimeter, and width of α-syn overexpressing dopamine neurons, to the level measured in naive untreated neurons shown in Figure 6 B-M (naive n = 190, α-syn n = 114 and α-syn + quinpirole n = 32, from at least three independent replicates; circularity: naive vs. α-syn p = 0.0021, naive vs. α-syn + quinpirole p = 0.4452, and α-syn vs. α-syn + quinpirole p = 0.0046; outer perimeter: WT vs. α-syn p = 0.0001, WT vs. α-syn + quinpirole p = 0.2250, and α-syn vs. α-syn + quinpirole p = 0.0312; shape factor: naive vs. α-syn p = 0.0021, naive vs. α-syn + quinpirole p = 0.5574, and α-syn vs. α-syn + quinpirole p = 0.0086; width: naive vs. α-syn p = 0.0001, WT vs. α-syn + quinpirole p = 0.1419, and α-syn vs. α-syn + quinpirole p = 0.0187, one-way ANOVA followed by Tukey’s HSD).

Next, we examined the impact of α-syn overexpression on neuronal survival by counting TH-positive neurons via immunocytochemistry. Compared to naive neurons, we found significantly fewer TH positive neurons following α-syn overexpression; quinpirole-mediated activation of D2 receptors (0.5 μM for 48 hours) prevented the neuronal loss (Fig 6 N: WT vs. α-syn p = 0.0008, WT vs. α-syn + quinpirole p = 0.1364, and α-syn vs. α-syn + quinpirole p = 0.0021, from three independent biological replicates, one-way ANOVA followed by Tukey’s HSD). The increased neuronal survival following quinpirole pretreatment is consistent with previous reports[93,101–104] and support the interpretation

that there is a correlation between α-syn modulation of neuronal complexity, neuronal vulnerability, and neuronal loss[109–111]. Neuronal survival is not equivalent to neuronal viability. While these data suggest pretreatment with a D2 receptor agonist increases neuronal survival following α-syn overexpression, they do not demonstrate a restoration of neuronal activity. Therefore, next, we asked whether quinpirole pretreatment prevents the perpetual increase in action potential frequency, increased intra- and extracellular dopamine levels, and elevated intraneuronal calcium dynamics in α-syn overexpressing neurons.

D2 receptor activation partially restores neuronal activity in α-synuclein-overexpressing dopamine neurons. The energy homeostasis principle suggests, the balance between energy income, expenditure, and availability are the key parameters in determining neuronal endurance[112]. Action potentials impose the highest energy demands on neurons[88,112,113]. In addition, dopamine metabolism is strongly linked to oxidative stress, as its degradation generates reactive oxygen species[13,114,115] that have shown to increase the vulnerability of dopamine neurons to oxidative stress[87,115–121]. So far, we have identified multiple interrelated mechanisms that would add fuel to vulnerability of α-syn overexpressing dopamine neurons. We identified a perpetual increase in action potential frequency, increased intra- and extracellular dopamine levels, and elevated intraneuronal calcium dynamics in α-syn overexpressing neurons, that are directly or indirectly related to decreased D2R activity. The unexpected observation that bath application of D2R agonist increased neuronal survival and nearly restored neuronal complexity of α-syn overexpressing neurons to the levels measured in naive dopaminergic neurons at baseline, suggests pharmacological activation of D2 receptors might be a possible target to alleviate the untoward consequences of α-syn overexpression on neuronal activity prior to neuronal death. To test this hypothesis, we treated α-syn overexpressing neurons with 0.5 μM quinpirole for 48 hours before assessing calcium dynamics, spontaneous firing activity, and dopamine release and synthesis in these neurons (Figure 7). This data is compared to the previous data which is overlaid with a black dotted line that represents the average values measured for untreated naive neurons and the pink dotted line represents the average values for untreated α-syn overexpressing neurons. We found that a prolonged D2R activation partially restores calcium dynamics in these neurons, approximating calcium dynamics measured in untreated naive neurons (Figure 7 A-F, n = 28 quinpirole treated α-syn overexpressing neurons, two-tailed unpaired t-test, α-syn vs. α-syn pretreated with quinpirole $p = 0.2024$ event rate, $p = 0.0277$ event widths, $p = 0.6204$ event height), suggesting a restoration of calcium homeostasis in these neurons that might be causal or a consequence of a shift in neuronal activity. To test this hypothesis, we employed whole-cell current clamp recordings to measure the spontaneous firing activity of α-syn overexpressing neurons after treatment with quinpirole (0.5 μM for 48 hours). Quinpirole pretreatment on α-syn overexpressing neurons decreased the burst firing frequency, shortened the intermediated periods of quiescence and restored firing regularity, near the values measured in untreated naive neuron's firing pattern (Figure 7G-K, n = 7 from three independent biological replicates, 1.325 ± SEM for quinpirole-treated α-syn overexpressing neurons, two-tailed unpaired t-test, α-syn vs. α-syn pretreated with quinpirole $p = 0.0342$ for firing frequency, $p = 0.1053$ for ISI, $p = 0.4778$ for CV of ISI).

These results suggest that dysregulation of D2 receptor in α-syn overexpressing dopamine neurons can be partially rescued with prolonged activation of the remaining functional D2 receptors on the cell surface

The observed changes in neuronal responses and calcium activity following extended D2 receptor activation could be predictive of downstream changes in dopamine synthesis in α-syn overexpressing neurons. To test the hypothesis that D2 receptor activation decreases α-syn modulation of dopamine release, we measured extracellular dopamine levels via two complementary approaches: live-cell imaging and HPLC. To measure D2R-mediated modulation of baseline extracellular dopamine levels (0.5 μM quinpirole 48 hours) in α-syn overexpressing neurons, we co-cultured $GRAB_{DA4.4}$-expressing cells with the quinpirole-treated, α-syn overexpressing dopamine neurons for 20-24 hours prior to imaging. Quinpirole pretreatment of α-syn overexpressing neurons decreased basal $GRAB_{DA4.4}$ fluorescence (used as a proxy to measure basal dopamine release) around the soma and dendritic fields (Figure 7 L, M), comparable to values measured in naive untreated neurons shown in Figure 4 (black dotted line in Figure 7). Consistent with the literature [36,54,122–125], quinpirole silenced naive dopamine neurons and decreased basal extracellular dopamine (n = 6 from three independent replicates; data shown as ±SEM, one-way ANOVA followed by Tukey's HSD, naive vs. α-syn treated with quinpirole p = 0.9948, α-syn vs. α-syn treated with quinpirole p = 0.0003).

As a complementary approach, via a double-blinded experimental design, we used HPLC, as described in the Methods and in Figure 4, to measure extracellular dopamine level in the external milieu of neurons after quinpirole pretreatment (0.5 μM for 48 hours). HPLC analysis revealed a reduction in basal dopamine release in all quinpirole-treated experimental groups, with the largest fold decrease in α-syn overexpressing neurons (Figure 7 N, n = 3 from independent biological replicates, one-way ANOVA followed by Tukey's HSD, α-syn vs. α-syn treated with quinpirole p = 0.0325 and naive vs. α-syn treated with quinpirole p = 0.9959;). Therefore, through pharmacological manipulation of D2 receptors, the α-syn dysregulation of dopamine transmission is potentially reversible (n = 3 each, from 3 independent biological replicates, one-way ANOVA followed by Tukey's HSD, α-syn vs. α-syn treated with quinpirole p = 0.0325 and naive vs. α-syn treated with quinpirole p = 0.9959). The restoration of extracellular dopamine could be due to decreased neuronal activity, decreased dopamine synthesis, or both. Since we have already examined the former (Figure 7A-K), to test the possibility of decreased dopamine synthesis, we used HPLC to measure intracellular dopamine levels via a double-blinded experimental design (described in Methods). Intracellular dopamine levels in quinpirole-treated α-syn overexpressing neurons were significantly reduced compared to untreated α-syn overexpressing neurons (Figure 7O, n = 3 independent biological replicates, one-way ANOVA followed by Tukey's HSD, α-syn vs. α-syn treated with quinpirole p = 0.0449 and naive vs. α-syn treated with quinpirole p = 0.6197) shown in Figure 4 (pink dotted line; n = 3 each, from 3 independent replicates, one-way ANOVA followed by Tukey's HSD, α-syn vs. α-syn treated with quinpirole p = 0.0325 and WT vs. α-syn treated with quinpirole p = 0.9959). Since activation of D2R negatively regulates tyrosine hydroxylase[35,36,66,75,76,124,126,127] and neuronal activity[33–36,38,39], we then tested the hypothesis that reduced intra- and extracellular dopamine are, in part, due to decreased

TH protein levels. Via a double-blinded experimental design, we utilized quantitative ELISA, as described in Figure 4, to measure TH levels. As shown in Figure 7P, TH protein level is decreased in quinpirole-treated, α-syn overexpressing neurons compared to untreated (0.5 μM for 48 hours; n = 3, one-way ANOVA followed by Tukey's HSD, WT vs. α-syn treated with quinpirole p = 0.4288 and α-syn vs. α-syn treated with quinpirole p = 0.6809). The partial rescue of α-syn-induced neuronal dysregulation after D2R activation is consistent with neuroprotective properties of D2 receptors described previously[104,128–131]. It has been shown that D2 autoreceptors suppress dopamine synthesis through a negative feedback mechanism, and thus reduce oxidative stress caused by a high level of cytoplasmic dopamine[128–130]. In addition, consistent with our data, activation of D2 autoreceptors mediates neuroprotection by reducing neuronal excitability, cytoplasmic dopamine, and calcium levels[104,131] that can restore the balance between energy income, expenditure, and its availability[112]. The data presented in this study provide a potential druggable target that may revert or prevent the untoward consequences of α-syn burden on dopamine neuronal viability and activity.

Concluding remarks

In this study, we found α-syn overexpression dysregulates the structural and functional properties of dopaminergic neurons. The untoward consequences of increased α-syn likely cascade across the neuron, protracting the neuronal processes, increasing calcium burdens and biophysical properties of dopamine neurons as measured by increased burst firing activity. We found that the endogenous self-regulation of dopaminergic neurons fails to restrain the exacerbation of these phenotypes. Thereby, the signaling of these neurons in their networks becomes erratic, potentially creating avalanching neuronal dysfunction. The dysregulation of dopamine signaling within the brain therefore precedes neuronal demise. However, we show that these progressive dysregulations can be reversed through pharmacological manipulation.

D2 autoreceptors feedback mechanism is one of the main autoinhibitory mechanisms regulating dopamine neuronal activity[36,38,132]. We found D2 autoreceptors activity is diminished in α-syn overexpressing dopamine neurons, and prolonged incubation with a D2 receptor agonist, quinpirole (48 hours, 0.5 μM), nearly restored the firing activity to its canonical levels, reinstated intra and extracellular dopamine levels, and prevented losses in neuronal demise and structural neural complexity. Notably, D2 receptor agonists (full and partial) have attained FDA approval and have made their way into the clinic; however, these are often tested in late-stage PD. Our results suggest that the current treatment timeline may occur too late and that the efficacy of this strategy requires early intervention to reduce the rate of neuronal demise. Most crucially, our results suggest that neuronal loss is preventable and with future exploration across other mechanistic pathways in addition to D2 receptor pharmacology will reveal intersectional treatments that may have the capacity to ameliorate PD.

Materials and Methods

The experiments in this study are performed via a blinded or when possible double-blinded experimental design.

Reagents and chemicals: The source, catalogue number and concentration of reagents, antibodies and chemicals used in this study are outlined in Table 1. All viral vectors utilized in this study are listed in Table 2.

Animals: All experiments were approved by the Institutional Animal Care and Use Committee at University of Florida. Mice were housed in the animal care facility at the University of Florida, 2-4 per cage with food and water available ad libitum in the home cage. The room was maintained under 12-hour light/dark cycle. Wild-type C57BL/6J mice, or DAT^{IREScre} and Ai95(RCL-GCaMP6f)-D (Ai95D) knock-in mice were obtained from The Jackson Laboratory (Stock number: 006660 (DAT^{IREScre}), 024105 (Ai95D), Bar Harbor, ME, USA). WT pups, or pups expressing GCaMP6f in dopamine neurons were used for this study. Mice of both sexes were used.

AAV1-TH-α-synuclein and AAV1-TH-GFP generation: The pAAV2.5-THP-GFP plasmid was purchased from Addgene (#80336)[133]. Human α-synuclein cDNA from a pcDNA3.1 plasmid was restriction digested with EcoRI and HindIII (NEB), purified and ligated in the same sites of the pAAV2.5-THP backbone to generate the pAAV2.5-TH- α-syn plasmid. Purified pAAV2.5TH- α-syn and pAAV2.5-TH-GFP vectors were utilized to prepare active AAV (capsid 1) using a HEK293T-based transfection method followed with iodixanol gradient purification as previously described [134] and these virus were termed AAV1-TH-α-syn and AAV1-TH-GFP. Genomic titer of each virus was assayed by quantitative PCR as previously described[134].

Primary Neuronal Culture: Primary culture was prepared as previously described, with small distinctions [50]. Briefly, acutely dissociated mouse midbrains from 0-2-day old male and female pups were isolated and incubated in dissociation medium at 35–37 °C under continuous oxygenation for 60-90 min. Dissociated cells were triturated with pipettes of decreasing bore size (including a punctured fire-polished pipette), then pelleted by centrifugation at 1500 rpm for 3-5 min, and resuspended and plated in glial medium (Table 1). Cells were plated at a density of 100,000 cells/coverslip, on 12 mm coverslips coated with 0.1 mg/ml poly-D-lysine and 5 µg/ml laminin and maintained in neuronal media. After 2 hours, cells were supplemented with neuronal media (DIV0 composition). Every 4 days, half of the media was replaced with fresh media. On DIV5, cultures were transduced with the desired AAV1 (see Table 2). The experiments described in this study were performed on DIV9-11. Reagents and chemicals utilized for midbrain neuronal culture are listed in Table 1.

Electrophysiology: Spontaneous firing activity of midbrain dopamine neurons was examined via whole cell current clamp recordings as previously described[46,48,51]. The neurons were continuously perfused with ACSF (composition described in Table 1) equilibrated with 95% O2/5% CO_2; pH was adjusted to 7.4 at 37 °C. Patch electrodes were fabricated from borosilicate glass (Cat. No. 1B150F-4,1.5 mm outer diameter; World Precision Instruments, Sarasota, FL) with the P-2000 puller (Sutter Instruments, Novato, CA). The tip resistance was in the range of 3-5 MΩ. The electrodes were filled with a pipette solution containing (in mM): 120 potassium gluconate, 20 KCl, 2 $MgCl_2$, 10 HEPES, 0.1 EGTA, 2 ATP, and 0.25 GTP, with pH adjusted to 7.25 with KOH. All

experiments were performed at 37 °C. To standardize action potential (AP) recordings, neurons were held at their resting membrane potential (see below) by DC application through the recording electrode. Action potential was recorded if the following criteria were met: a resting membrane potential more polarized than −35 mV and an action potential peak amplitude greater than 60 mV. Action potential half-width was measured as the spike width at the half-maximal voltage using Clampfit 10 software (Molecular Devices LLC, San Jose, CA). Steady-state basal activity was recorded for 2–3 min before bath application of the drug. Each coverslip was used for only one recording, this is specifically important for experiments involving drug application. The spontaneous spike activity of midbrain dopamine neurons was obtained by averaging 1 min interval activities at baseline and after 3-5 min of drugs.

Live Cell Calcium Imaging: *These experiments were performed via a blinded experimental design.* Live cell calcium imaging and analysis are described previously[50]. Briefly, naive (non-transduced) and α-syn overexpressing (transduced with AAV1-TH-α-synuclein) midbrain neuronal cultures were imaged with a Nikon Eclipse FN1 upright microscope (Nikon Instruments, Melville, NY). A Spectra X (Lumencor, Inc, Beaverton, OR) was used to stimulate GCaMP6f (λ_{ex} = 470 nm) fluorescence through a custom quad-pass filter (Chroma Technologies, Battleboro, VT), and emission was filtered through visible spectra bandpass filter. Experiments were performed under gravity perfusion of artificial cerebral spinal fluid (ACSF, Table 1). The average fluorescence of the first 60s recording is defined as baseline. After baseline imaging, vehicle (ACSF), 1 μM DA, or 10 μM quinpirole was administered via a perfusion system (flow rate of 2 ml/min) and recorded for additional 2 minutes. Neuronal somatic regions of interest (ROI) were auto detected for the cell body of each individual neuron. Background fluorescence was subtracted from each frame. Fold fluorescence change from baseline was calculated and plotted against time. Each coverslip was used for only one recording, this is specifically important for experiments involving drug application. All resources and reagents used for live cell calcium imaging experiments are listed in Table 1.

Live cell confocal imaging using $GRAB_{DA4.4}$- expressing HEK 293 cells to measure *extracellular dopamine:* *These experiments were performed via a double-blinded experimental design.* $GRAB_{DA4.4}$ is a genetically encoded fluorescent dopamine sensor, engineered by coupling a conformationally-sensitive circular-permutated EGFP (cpEGFP) to D2 receptor. In $GRAB_{DA4.4}$-expressing HEK293 cells, dopamine binding to the sensor induces a conformational change which results in a robust increase in fluorescence signal via a concentration-dependent manner [135]. Flp-In™ 293 T-Rex stable cell lines exhibiting tetracycline-inducible expression of the $GRAB_{DA4.4}$ dopamine sensor was generously gifted by Dr. Ulrik Gether. The $GRAB_{DA4.4}$- expressing HEK 293 cells were maintained in DMEM supplemented with 10% FBS and 100 units/ml Penicillin/Streptomycin. Selection pressure for $GRAB_{DA4.4}$ expressing cells was maintained with media containing Hygro-B (1 mg/ml) and Blasticidin (0.015 mg/ml). The cells were plated on coverslips in media containing tetracycline (1:1000) to induce expression for 12-24 hours before live cell imaging under three conditions: 1) only $GRAB_{DA4.4}$-expressing HEK293 cells, to measure constitutive fluorescent signal, 2) $GRAB_{DA4.4}$ cells added to tdTomato expressing dopaminergic neurons, 3) $GRAB_{DA4.4}$ cells

added to tdTomato expressing dopamine neurons overexpressing α-syn. The tdTomato transduction (λ_{ex} = 560 nm) is used for a better identification of soma and dendritic field and no fluorophore overlap (i.e. excitation and emission of tdTomato does not bleed through GFP channel). Imaging was performed using a Nikon Eclipse FN1 upright microscope (Nikon Instruments, Melville, NY). A Spectra X (Lumencor, Inc, Beaverton, OR) was used to stimulate GFP (λ_{ex} = 470 nm), tdTomato (λ_{ex} = 560 nm) fluorescence through a custom quad-pass filter (Chroma Technologies, Battleboro, Vermont). Emission was filtered through visible spectra bandpass filter. Regions of interest (ROI) were autodetected via NIS Elements software (Nikon Instruments, Melville, NY). cpEGFP signal was background subtracted using an ROI in an adjacent area of the image devoid of cells or debris.

Generation of standard curve: To generate a standard curve, the baseline fluorescence signal (Fc) which is the constitutive fluorescent signal in the absence of extracellular dopamine was recorded. Changes in fluorescence signal after adding various dopamine concentrations (1-20 nM) were plotted against dopamine concentration.

Measurement of basal dopamine release: $GRAB_{DA4.4}$ cells are co-cultured with tdTomato expressing dopamine neurons ($DAT^{IRES\,cre}$-LoxP-tdTomato) containing endogenous α-syn or its overexpression 20-24 hours prior to live cell confocal imaging. At the beginning of each experiment, the constitutive $GRAB_{DA4.4}$ fluorescence signal (F_c) of the cells that are plated in similar conditions sans neurons was obtained. To compare baseline dopamine release amongst the experimental groups, the average ratio of fluorescence signal of cells adjacent to the soma and neuronal processes to the average ratio of fluorescence signal of $GRAB_{DA4.4}$ cells (only) were calculated ($F_{baseline}$ = ($F_{GRAB\ DA4.4\ cells\ grown\ with\ neurons}$ – F_c) / F_c).

Visualization and quantification of real-time dopamine release following KCl stimulation. 20-24 hours prior to live cell confocal imaging, $GRAB_{DA4.4}$ cells are co-cultured with tdTomato expressing dopamine neurons containing endogenous α-synuclein or its overexpression. $GRAB_{DA4.4}$ fluorescent signal around the soma and neuronal processes were measure before ($F_{baseline}$) and following KCl-stimulation (90 mM) of dopamine release [57]. Average fluorescence signal of cells adjacent to the soma and neuronal processes before and after KCl were calculated ($\Delta F/F$ = ($F_{stimulated}$ – $F_{baseline}$) / $F_{baseline}$).

Immunocytochemistry (ICC): *These experiments were performed via a double-blinded experimental design.* On DIV9-11, naive (non-transduced) and α-syn overexpressing neuronal cultures were fixed with 4% paraformaldehyde (PFA) in PBS for 30 min at room temperature (RT), followed by blocking, permeabilization and overnight incubation (at 4 °C) with primary antibodies diluted in blocking buffer, followed by three 20-min phosphate buffer solution (PBS) washes. Then, a 1-hour incubation in blocking buffer with Alexa-Fluor conjugated secondary antibodies at RT, followed by three 20-min washes and an overnight PBS wash at RT. Coverslips were mounted on slides using Fluoromount-G. Images were captured on a Nikon A1 laser-scanning confocal microscope (20X or 40X oil-immersion objective). Reagents and chemicals utilized for ICC are listed in Table 1.

Western Blot Analysis: *These experiments were performed via a double-blinded experimental design.* For detection of endogenous and human α-syn total cell lysate of

neurons transduced with AAV1-TH-α-syn (n = 4) or naive (non-transduced) neurons (n = 4) were used, as described previously [136]. Briefly, the cells were harvested in 200 µL of 2% SDS buffer, protein concentrations were determined using the bicinchoninic acid assay (Pierce), and further diluted in sample buffer (10 mM Tris, pH 6.8, 1 mM EDTA, 40 mM DTT, 0.005% Bromophenol Blue, 0.0025% Pyronin Yellow, 1% SDS, 10% sucrose). Following harvest of total cell lysate, samples were heated to 100 °C for 10 minutes prior to SDS-PAGE (13% polyacrylamide gels, 10 µg lysate per well) followed by electrophoretic transfer onto 0.2 µm nitrocellulose membranes as previously described [136]. Membranes were incubated with block solution (5% milk in TBS) for 1 h, then with primary antibodies (in block solution) overnight at 4°C. Membranes were washed with TBS-T and incubated with goat anti-mouse or anti-rabbit secondary antibodies conjugated to horseradish peroxidase (Jackson Immuno Research Labs, Westgrove, PA) diluted in block solution at room temperature for 1 hour. Immunoreactivity was assessed using Western Lightning-Plus ECL reagents (PerkinElmer, Waltham, MA) followed by chemiluminescence imaging (Genegnome XRQ, Syngene, Frederick, MD). For α-syn detection we used 94-3A10 antibody, which is a mouse monoclonal antibody raised against C-terminal regions (130-140) of α-syn [137]. For loading control, we used mouse monoclonal anti-actin C4 antibody (EMD Millipore). For tyrosine hydroxylase detection, an affinity purified rabbit antibody AB152 (EMD Millipore) was used.

Biotinylation Assay: *These experiments were performed via a double-blinded experimental design.* α-Syn overexpressing neuronal cultures and non-transduced neuronal cultures were washed three times with cold PBS and incubated with sulfo-NHS-biotin (1.5 mg/ml; ThermoFisher Pierce, 21331) for 30 minutes at 4 °C with rocking. Remaining sulfo-NHS-biotin was quenched with cold Quenching Solution (Glycine 50 mM in PBS), followed by three washes with cold PBS[138,139]. Cells were lysed in BufferD lysis buffer (10% Glycerol, 125 mM NaCl, 1 mM EDTA, 1 mM EGTA, pH 7.6) containing 1% Triton-X100 and protease inhibitor cocktail (Millipore, 539131) for 1 hour at 4 °C with rocking, followed by centrifugation for 15 minutes at 12,000 g. The supernatants were divided into three portions – 25 µl for protein quantification, 200 µl for incubation with Avidin, with the remainder for whole lysate. After equilibrating monomeric UltraLink Avidin (ThermoFisher Pierce, 53146) twice with 1 ml BufferD, 40 µl of 50% bead slurry were added to 200 µl lysate and incubated at 4 °C for 1 hour with rotation. Supernatant was retained as cytoplasmic fraction, and beads were washed three times with 1 ml BufferD, eluted with 40 µl Laemmli Sample Buffer 4x (containing 10% beta-mercaptoethanol) at 37 °C for 30 minutes and separated by 10% SDS-PAGE, transferred to 0.45 µm nitrocellulose and probed with antibodies against proteins of interest (see Table 1). Fluorescent images were analyzed using ImageJ (NIH) to measure band optical density. Values were normalized to total protein per lane. Beta-tubulin (Aves, TUJ) was probed to demonstrate membrane fraction isolation during biotinylation.

ELISA Quantification of Tyrosine Hydroxylase (TH): *These experiments were performed via a double-blinded experimental design.*
Cell lysis: For total protein quantification via ELISA, neuronal cultures were washed three times with cold PBS, then lysed in BufferD lysis buffer (10% Glycerol, 125 mM NaCl, 1 mM EDTA, 1 mM EGTA, pH 7.6) containing 1% Triton-X100 and protease inhibitor

cocktail (Millipore, 539131) for 1 hour at 4 °C with rocking, followed by centrifugation for 15 minutes at 12,000g. Samples were denatured in Laemmli Sample Buffer 4x (containing 10% beta-mercaptoethanol) at 37 °C for 30 minutes and separated by 10% SDS-PAGE, transferred to 0.45 µm Nitrocellulose and probed with antibodies against proteins of interest. Values were normalized to total protein per lane.

TH ELISA: Antibodies and concentrations used are given in Table 1. In brief, Immulon 4 HBX High-Binding 96 well plates were coated with 100 µl per well of 1:1,000 dilution of mouse anti-TH (EnCor, MCA-4H2) in coating buffer (28.3 mM Na_2CO_3, 71.42 mM $NaHCO_3$, pH 9.6) for 20 hours at 4 °C. Edge lanes 1 and 12 were left empty. Wells were blocked with 5% fat free milk in 1x TBS (pH 7.4) for 1 hour at room temperature on an orbital shaker set to 90rpm.

Generation of standard curve: To produce a standard curve, two standard curve lanes were generated, with six serial dilutions, beginning at 10 ng/ml and 1 ng/ml in TBS-T containing 1% fat free milk (with the last well in each standard curve lane left with incubation buffer only as a blank. Remaining wells were incubated in duplicate with lysates from cells of interest. Incubation was completed for 20 hours at 4 °C on an ELISA shaker set to 475 rpm. After each well was washed and aspirated 6 times with TBS-T, anti-TH rabbit (EnCor, RPCA-TH) conjugated to biotin was dilute 1:6,000 from a stock concentration of 1.65 mg/ml in TBS-T with 1% fat-free milk and incubated for 1 hour at room temperature at 425 rpm. 100 µl Avidin-HRP (Vector labs, A-2004), diluted 1:2,500 in TBS-T with 1% fat-free milk, was added to each well following wash, and incubated for 1 hour at room temperature at 425 rpm. Following final washes, 150 µl room temperature TMB-ELISA reagent (Thermo Fisher, 34028) was added to each well. The reaction was allowed to continue for 20 minutes, protected from light, and stopped by addition of 50 µl 2N H_2SO_4. The plate was immediately read at 450 nm. Duplicate standard and sample wells were averaged, and background-subtracted based on blank wells. TH Concentration was calculated using a quadratic curve equation calculated in Graphpad Prism 8, then normalized to total protein concentration per sample as calculated using Lowry Assay. Final TH values shown are presented as pg TH/mg total protein after multiplication of the nanogram TH value by 1,000 to show TH as picogram TH/milligram total protein.

HPLC: *These experiments were performed via a double-blinded experimental design.* Midbrain primary cultures were incubated in KH buffer (Table 1), at 37 °C, for 1 hour before collecting intracellular and extracellular milieu for HPLC analysis [140,141]. For extracellular milieu, KH buffer incubated with neurons was collected, treated with 1M perchloric acid and snap frozen for analysis. For intracellular milieu, coverslips were washed with KH buffer, scraped, and treated with 1M perchloric acid, before sonicating. Then sample was centrifuged at 12000 rpm at 4°C for 10 min, and supernatant snap-frozen in liquid nitrogen for analysis. The pellet was resuspended using 0.2 NaOH and RIPA buffer[142] for protein quantification via Lowry assay. Samples were centrifuged at 16,000 g for 15 min (4°C) and the supernatant was filtered through a 0.2 mm pore membrane (Nanosep with 0.2 mm bioinsert, Pall Life Sciences) and 15 µl of the supernatant was injected directly into an HPLC-ECD (HTEC-510; Eicom). Dopamine was separated on a CAX column (EICOMPAK 2.0 id x 200 mm) maintained at 35°C. The mobile phase consisted of 70% 0.1 M ammonium acetate buffer (pH 6.0) containing

sodium sulfate (0.025 M), EDTA-2Na (50 mg/l) and 30% methanol at a flow rate of 250 µl/min. An electrochemical detector that used a glassy working electrode (+ 450 mV) against a silver-silver chloride reference electrode (WE-3G; Eicom) was used to quantify dopamine in the samples. A dopamine standard was used to identify and quantify the dopamine concentration in the samples.

Morphometric Analysis: *These experiments were performed via a double-blinded experimental design.* Control ($DAT^{IRES cre}$) neurons and α-syn overexpressing neurons ($DAT^{IRES cre}$/α-syn) were transduced with AAV1-LoxP-tdTomato (Addgene) on DIV5. Neurons were fixed with 4% paraformaldehyde for 30 minutes at room temperature on DIV10, and coverslips were mounted using Fluoromount-G and allowed to dry. Alternatively, neurons were fixed, co-immunolabeled with TH and GFP antibodies, and mounted for imaging, as described above. Images were captured on a Nikon A1 laser-scanning confocal microscope (visualized through a 20X oil-immersion objective). Images of neurons with minimal interference from neighboring neurons were analyzed in ImageJ (FIJI) and converted to 8-bit binary images after threshold adjustment. Sholl analysis plugin was used to draw concentric circles starting from 15 µm followed by 5 µm successive shells in order to identify the number of intersections along the radii[94,143,144]. Sholl analysis was performed and the number of intersections were plotted (Figure 6). Cell area measurements were attained by manually drawing ROI around cell soma using the free polygon selection tool in ImageJ. ROIs were drawn to encompass the complete projection area of the cell and selection was finalized by convex hull to attain final projection area measurement. Results obtained were plotted to analyze complexity of morphology in non-transduced controls and *α-synuclein*-expressing neurons.

Statistical Analysis: Data analysis was performed using Graphpad Prism version 8.02 and MATLAB version 2020a. Student's t-test, linear regression, one-way, two-way, or repeated measures ANOVA were used where appropriate and corrected for multiple comparisons. Significance of $P < 0.05$ was considered statistically significant. Data are presented with mean and standard error unless otherwise stated.

Contributions

H.K. and B.G. conceived and supervised the study. H.K., B.G., A.D., D.R.M, A.G., Z.A.S. and J.J.L. designed and planned the experiments. A.D., D.R.M., F.S., M.L., A.G., S.H., Z.A.S., and J.J.L. collected the data. A.D., D.R.M., S.V., A.R.A., J.A., and C.A.H. analyzed the data. H.K., B.G., A.D., and D.R.M. interpreted the data with comments from N.U. H.K., B.G., A.D., and D.R.M. prepared the manuscript. B.U. and A.M.B. revised the work.

Competing interests

The authors declare no competing interests.

References

1. Cenci, M. A. Dopamine dysregulation of movement control in l-DOPA-induced dyskinesia. *Trends in Neurosciences* **30**, 236–243 (2007).

2. Panigrahi, B. *et al.* Dopamine Is Required for the Neural Representation and Control of Movement Vigor. *Cell* **162**, 1418–1430 (2015).

3. Braak, H. & Braak, E. Pathoanatomy of Parkinson's disease. in *Journal of Neurology, Supplement* **247**, 3–10 (Springer, 2000).

4. Burke, R. E., Dauer, W. T. & Vonsattel, J. P. G. A critical evaluation of the Braak staging scheme for Parkinson's disease. *Annals of Neurology* **64**, 485–491 (2008).

5. Goedert, M., Spillantini, M. G., Del Tredici, K. & Braak, H. 100 years of Lewy pathology. *Nature Reviews Neurology* **9**, 13–24 (2013).

6. Uchihara, T. & Giasson, B. I. Propagation of alpha-synuclein pathology: hypotheses, discoveries, and yet unresolved questions from experimental and human brain studies. *Acta Neuropathologica* **131**, 49–73 (2016).

7. Delenclos, M. *et al.* Neonatal AAV delivery of alpha-synuclein induces pathology in the adult mouse brain. *Acta Neuropathol. Commun.* **5**, 51 (2017).

8. Chartier-Harlin, M. C. *et al.* α-synuclein locus duplication as a cause of familial Parkinson's disease. *Lancet* **364**, 1167–1169 (2004).

9. Singleton, A. B. *et al.* α-Synuclein Locus Triplication Causes Parkinson's Disease. *Science (80-.).* (2003). doi:10.1126/science.1090278

10. Croisier, E., Moran, L. B., Dexter, D. T., Pearce, R. K. B. & Graeber, M. B. Microglial inflammation in the parkinsonian substantia nigra: Relationship to alpha-synuclein deposition. *J. Neuroinflammation* **2**, 14 (2005).

11. St Martin, J. L. *et al.* Dopaminergic neuron loss and up-regulation of chaperone protein mRNA induced by targeted over-expression of alpha-synuclein in mouse substantia nigra. *J. Neurochem.* **0**, 070214184024010-??? (2007).

12. Emanuele, M. & Chieregatti, E. Mechanisms of alpha-synuclein action on neurotransmission: Cell-autonomous and non-cell autonomous role. *Biomolecules* **5**, 865–892 (2015).

13. Dias, V., Junn, E. & Mouradian, M. M. The role of oxidative stress in parkinson's disease. *Journal of Parkinson's Disease* **3**, 461–491 (2013).

14. Outeiro, T. F. & Lindquist, S. Yeast Cells Provide Insight into Alpha-Synuclein Biology and Pathobiology. *Science (80-.).* **302**, 1772–1775 (2003).

15. Pereira, C., Bessa, C., Soares, J., Leão, M. & Saraiva, L. Contribution of Yeast Models to Neurodegeneration Research. *J. Biomed. Biotechnol.* **2012**, (2012).

16. Larsen, K. E. *et al.* α-Synuclein overexpression in PC12 and chromaffin cells impairs catecholamine release by interfering with a late step in exocytosis. *J. Neurosci.* **26**, 11915–11922 (2006).

17. Volles, M. J. & Lansbury, P. T. Relationships between the Sequence of α-Synuclein and its

Membrane Affinity, Fibrillization Propensity, and Yeast Toxicity. *J. Mol. Biol.* **366**, 1510–1522 (2007).

18. McBurney, R. N. & Neering, I. R. Neuronal calcium homeostasis. *Trends Neurosci.* **10**, 164–169 (1987).

19. Gleichmann, M. & Mattson, M. P. Neuronal calcium homeostasis and dysregulation. *Antioxidants and Redox Signaling* **14**, 1261–1273 (2011).

20. Grienberger, C. & Konnerth, A. Imaging Calcium in Neurons. *Neuron* **73**, 862–885 (2012).

21. Neher, E. & Sakaba, T. Multiple Roles of Calcium Ions in the Regulation of Neurotransmitter Release. *Neuron* **59**, 861–872 (2008).

22. Ekstrand, M. I. & Galter, D. The MitoPark Mouse - An animal model of Parkinson's disease with impaired respiratory chain function in dopamine neurons. *Park. Relat. Disord.* **15**, S185–S188 (2009).

23. Ricke, K. M. *et al.* Mitochondrial dysfunction combined with high calcium load leads to impaired antioxidant defense underlying the selective loss of nigral dopaminergic neurons. *J. Neurosci.* **40**, 1975–1986 (2020).

24. Angelova, P. R. *et al.* Ca2+ is a key factor in α-synuclein-induced neurotoxicity. *J. Cell Sci.* **129**, 1792–1801 (2016).

25. Augustine, G. J., Santamaria, F. & Tanaka, K. Local calcium signaling in neurons. *Neuron* **40**, 331–346 (2003).

26. Berridge, M. J., Bootman, M. D. & Roderick, H. L. Calcium signalling: Dynamics, homeostasis and remodelling. *Nature Reviews Molecular Cell Biology* **4**, 517–529 (2003).

27. Neher, E. & Sakaba, T. Multiple Roles of Calcium Ions in the Regulation of Neurotransmitter Release. *Neuron* **59**, 861–872 (2008).

28. Zucker, R. S. Calcium- and activity-dependent synaptic plasticity. *Curr. Opin. Neurobiol.* **9**, 305–313 (1999).

29. Duda, J., Pötschke, C. & Liss, B. Converging roles of ion channels, calcium, metabolic stress, and activity pattern of Substantia nigra dopaminergic neurons in health and Parkinson's disease. *Journal of Neurochemistry* **139 Suppl**, 156–178 (2016).

30. Barzilai, A. & Melamed, E. Molecular mechanisms of selective dopaminergic neuronal death in Parkinson's disease. *Trends in Molecular Medicine* **9**, 126–132 (2003).

31. Catoni, C., Calì, T. & Brini, M. Calcium, dopamine and neuronal calcium sensor 1: Their contribution to Parkinson's disease. *Front. Mol. Neurosci.* **12**, (2019).

32. Mosharov, E. V. *et al.* Interplay between Cytosolic Dopamine, Calcium, and α-Synuclein Causes Selective Death of Substantia Nigra Neurons. *Neuron* **62**, 218–229 (2009).

33. Jackson, D. M. & Westlind-Danielsson, A. Dopamine receptors: Molecular biology, biochemistry and behavioural aspects. *Pharmacology and Therapeutics* **64**, 291–370 (1994).

34. Paladini, C. A., Robinson, S., Morikawa, H., Williams, J. T. & Palmiter, R. D. Dopamine controls the firing pattern of dopamine neurons via a network feedback mechanism. *Proc. Natl. Acad. Sci. U.*

S. A. **100**, 2866–2871 (2003).

35. Beaulieu, J. M. & Gainetdinov, R. R. The physiology, signaling, and pharmacology of dopamine receptors. *Pharmacological Reviews* **63**, 182–217 (2011).

36. Ford, C. P. The role of D2-autoreceptors in regulating dopamine neuron activity and transmission. *Neuroscience* **282**, 13–22 (2014).

37. Bozzi, Y. & Borrelli, E. Dopamine in neurotoxicity and neuroprotection: What do D2 receptors have to do with it? *Trends in Neurosciences* **29**, 167–174 (2006).

38. Beckstead, M. J., Grandy, D. K., Wickman, K. & Williams, J. T. Vesicular dopamine release elicits an inhibitory postsynaptic current in midbrain dopamine neurons. *Neuron* **42**, 939–946 (2004).

39. Pucak, M. L. & Grace, A. A. Evidence that systemically administered dopamine antagonists activate dopamine neuron firing primarily by blockade of somatodendritic autoreceptors. *J. Pharmacol. Exp. Ther.* **271**, (1994).

40. Paul Kramer, A. F., Williams, J. T. & Kramer, P. F. Calcium Release from Stores Inhibits GIRK. *CellReports* **17**, 3246–3255 (2016).

41. Seabrook, G. R. *et al.* Depression of high-threshold calcium currents by activation of human D2 (short) dopamine receptors expressed in differentiated NG108-15 cells. *Br. J. Pharmacol.* **111**, 1061–1066 (1994).

42. Montmayeur, J. P. & Borrelli, E. Transcription mediated by a cAMP-responsive promoter element is reduced upon activation of dopamine D2 receptors. *Proc. Natl. Acad. Sci. U. S. A.* **88**, 3135–3139 (1991).

43. Missale, C., Russel Nash, S., Robinson, S. W., Jaber, M. & Caron, M. G. Dopamine receptors: From structure to function. *Physiological Reviews* **78**, 189–225 (1998).

44. Lee, A. K. Dopamine (D2) receptor regulation of intracellular calcium and membrane capacitance changes in rat melanotrophs. *J. Physiol.* **495**, 627–640 (1996).

45. Wei, C. *et al.* Response dynamics of midbrain dopamine neurons and serotonin neurons to heroin, nicotine, cocaine, and MDMA. *Cell Discov.* **4**, 60 (2018).

46. Sambo, D. O. *et al.* The sigma-1 receptor modulates methamphetamine dysregulation of dopamine neurotransmission. *Nat. Commun.* (2017).

47. Saha, K. *et al.* Intracellular methamphetamine prevents the dopamine-induced enhancement of neuronal firing. *J. Biol. Chem.* **289**, 22246–22257 (2014).

48. Lin, M., Sambo, D. & Khoshbouei, H. Methamphetamine Regulation of Firing Activity of Dopamine Neurons. *J. Neurosci.* **36**, 10376–10391 (2016).

49. Richardson, B. D. *et al.* Membrane potential shapes regulation of dopamine transporter trafficking at the plasma membrane. *Nat. Commun.* **7**, 10423 (2016).

50. Miller, D. R. *et al.* Methamphetamine regulation of activity and topology of ventral midbrain networks. *PLoS One* **14**, e0222957 (2019).

51. Saha, K. *et al.* Intracellular methamphetamine prevents the dopamine-induced enhancement of neuronal firing. *J. Biol. Chem.* **289**, 22246–22257 (2014).

52. Lin, M. *et al.* Mechanism of Manganese Dysregulation of Dopamine Neuronal Activity. *J. Neurosci.* **40**, 5871–5891 (2020).

53. Innis, R. B. & Aghajanian, G. K. Pertussis toxin blocks autoreceptor-mediated inhibition of dopaminergic neurons in rat substantia nigra. *Brain Res.* **411**, 139–143 (1987).

54. Lacey, M. G., Mercuri, N. B. & North, R. A. Dopamine acts on D2 receptors to increase potassium conductance in neurones of the rat substantia nigra zona compacta. *J. Physiol.* **392**, 397–416 (1987).

55. Kennedy, R. T., Jones, S. R. & Wightman, R. M. Dynamic Observation of Dopamine Autoreceptor Effects in Rat Striatal Slices. *J. Neurochem.* **59**, 449–455 (1992).

56. Brodie, M. S., Shefner, S. A. & Dunwiddie, T. V. Ethanol increases the firing rate of dopamine neurons of the rat ventral tegmental area in vitro. *Brain Res.* **508**, 65–69 (1990).

57. Jensen, K. L. *et al.* Pick1-deficient mice exhibit impaired response to cocaine and dysregulated dopamine homeostasis. *eNeuro* **5**, (2018).

58. Nieoullon, A., Cheramy, A. & Glowinski, J. Release of dopamine in vivo from cat substantia nigra [28]. *Nature* **266**, 375–377 (1977).

59. Hoffman, A. F. & Gerhardt, G. A. Differences in Pharmacological Properties of Dopamine Release Between the Substantia Nigra and Striatum: An In Vivo Electrochemical Study. *J. Pharmacol. Exp. Ther.* **289**, (1999).

60. Swant, J. *et al.* α-synuclein stimulates a dopamine transporter-dependent chloride current and modulates the activity of the transporter. *J. Biol. Chem.* **286**, 43933–43943 (2011).

61. Butler, B. *et al.* Dopamine transporter activity is modulated by α-synuclein. *J. Biol. Chem.* **290**, 29542–29554 (2015).

62. Lam, H. A. *et al.* Elevated tonic extracellular dopamine concentration and altered dopamine modulation of synaptic activity precede dopamine loss in the striatum of mice overexpressing human α-synuclein. *J. Neurosci. Res.* **89**, 1091–1102 (2011).

63. Lundblad, M., Decressac, M., Mattsson, B. & Björklund, A. Impaired neurotransmission caused by overexpression of α-synuclein in nigral dopamine neurons. *Proc. Natl. Acad. Sci. U. S. A.* **109**, 3213–3219 (2012).

64. Yavich, L. *et al.* Locomotor activity and evoked dopamine release are reduced in mice overexpressing A30P-mutated human α-synuclein. *Neurobiol. Dis.* **20**, 303–313 (2005).

65. Butler, B., Sambo, D. & Khoshbouei, H. Alpha-synuclein modulates dopamine neurotransmission. *Journal of Chemical Neuroanatomy* (2016). doi:10.1016/j.jchemneu.2016.06.001

66. Lindgren, N. *et al.* Dopamine D2 receptors regulate tyrosine hydroxylase activity and phosphorylation at Ser40 in rat striatum. *Eur. J. Neurosci.* **13**, 773–780 (2001).

67. Alerte, T. N. M. *et al.* α-Synuclein aggregation alters tyrosine hydroxylase phosphorylation and immunoreactivity: Lessons from viral transduction of knockout mice. *Neurosci. Lett.* **435**, 24–29 (2008).

68. Salvatore, M. F. & Pruett, B. S. Dichotomy of tyrosine hydroxylase and dopamine regulation

between somatodendritic and terminal field areas of nigrostriatal and mesoaccumbens pathways. *PLoS One* **7**, (2012).

69. Salvatore, M. F., Calipari, E. S. & Jones, S. R. Regulation of Tyrosine Hydroxylase Expression and Phosphorylation in Dopamine Transporter-Deficient Mice. *ACS Chem. Neurosci.* **7**, 941–951 (2016).

70. Salvatore, M. F., Garcia-Espana, A., Goldstein, M., Deutch, A. Y. & Haycock, J. W. Stoichiometry of tyrosine hydroxylase phosphorylation in the nigrostriatal and mesolimbic systems in vivo: Effects of acute haloperidol and related compounds. *J. Neurochem.* **75**, 225–232 (2000).

71. Dadalko, O. I. *et al.* mTORC2/rictor signaling disrupts dopamine-dependent behaviors via defects in striatal dopamine neurotransmission. *J. Neurosci.* **35**, 8843–8854 (2015).

72. Hakansson, K. *et al.* Regulation of striatal tyrosine hydroxylase phosphorylation by acute and chronic haloperidol. *Eur. J. Neurosci.* **20**, 1108–1112 (2004).

73. Onali, P., Mosca, E. & Olianas, M. C. Presynaptic dopamine autoreceptors and second messengers controlling tyrosine hydroxylase activity in rat brain. *Neurochem. Int.* **20**, 89–93 (1992).

74. El Mestikawy, S. & Hamon, M. Is Dopamine-Induced Inhibition of Adenylate Cyclase Involved in the Autoreceptor-Mediated Negative Control of Tyrosine Hydroxylase in Striatal Dopaminergic Terminals? *J. Neurochem.* **47**, 1425–1433 (1986).

75. Kehr, W., Carlsson, A., Lindqvist, M., Magnusson, T. & Atack, C. Evidence for a receptor-mediated feedback control of striatal tyrosine hydroxylase activity. *J. Pharm. Pharmacol.* **24**, 744–747 (1972).

76. WOLF, M. E. & ROTH, R. H. Autoreceptor Regulation of Dopamine Synthesis. *Ann. N. Y. Acad. Sci.* **604**, 323–343 (1990).

77. Beckstead, M. J. & Williams, J. T. Long-term depression of a dopamine IPSC. *J. Neurosci.* **27**, 2074–2080 (2007).

78. Barton, A. C., Black, L. E. & Sibley, D. R. Agonist-induced desensitization of D2 dopamine receptors in human Y-79 retinoblastoma cells. *Mol. Pharmacol.* **39**, (1991).

79. Salinas, A. G., Davis, M. I., Lovinger, D. M. & Mateo, Y. Dopamine dynamics and cocaine sensitivity differ between striosome and matrix compartments of the striatum. *Neuropharmacology* **108**, 275–283 (2016).

80. Davis, M. I. *et al.* The cannabinoid-1 receptor is abundantly expressed in striatal striosomes and striosome-dendron bouquets of the substantia nigra. *PLoS One* **13**, e0191436 (2018).

81. Gainetdinov, R. R., Premont, R. T., Bohn, L. M., Lefkowitz, R. J. & Caron, M. G. DESENSITIZATION OF G PROTEIN–COUPLED RECEPTORS AND NEURONAL FUNCTIONS. *Annu. Rev. Neurosci.* **27**, 107–144 (2004).

82. Robinson, B. G. *et al.* Desensitized D2 autoreceptors are resistant to trafficking. *Sci. Rep.* **7**, 1–14 (2017).

83. Krupnick, J. G. & Benovic, J. L. THE ROLE OF RECEPTOR KINASES AND ARRESTINS IN G PROTEIN–COUPLED RECEPTOR REGULATION. *Annu. Rev. Pharmacol. Toxicol.* **38**, 289–319 (1998).

84. Bartlett, S. E. *et al.* Dopamine responsiveness is regulated by targeted sorting of D2 receptors. *Proc. Natl. Acad. Sci. U. S. A.* **102**, 11521–11526 (2005).

85. Matsuda, W. *et al.* Single nigrostriatal dopaminergic neurons form widely spread and highly dense axonal arborizations in the neostriatum. *J. Neurosci.* **29**, 444–453 (2009).

86. Giguère, N. *et al.* Increased vulnerability of nigral dopamine neurons after expansion of their axonal arborization size through D2 dopamine receptor conditional knockout. *PLOS Genet.* **15**, e1008352 (2019).

87. Pacelli, C. *et al.* Elevated Mitochondrial Bioenergetics and Axonal Arborization Size Are Key Contributors to the Vulnerability of Dopamine Neurons. *Curr. Biol.* **25**, 2349–2360 (2015).

88. Bolam, J. P. & Pissadaki, E. K. Living on the edge with too many mouths to feed: Why dopamine neurons die. *Mov. Disord.* **27**, 1478–1483 (2012).

89. Ducrot, C. *et al.* Dopaminergic neurons establish a distinctive axonal arbor 1 with a majority of non-synaptic terminals 2 3. doi:10.1101/2020.05.11.088351

90. Kordower, J. H. *et al.* Disease duration and the integrity of the nigrostriatal system in Parkinson's disease. *Brain* **136**, 2419–2431 (2013).

91. Decressac, M., Mattsson, B., Lundblad, M., Weikop, P. & Björklund, A. Progressive neurodegenerative and behavioural changes induced by AAV-mediated overexpression of α-synuclein in midbrain dopamine neurons. *Neurobiol. Dis.* **45**, 939–953 (2012).

92. Chen, S. *et al.* D2/D3 receptor agonist ropinirole protects dopaminergic cell line against rotenone-induced apoptosis through inhibition of caspase- and JNK-dependent pathways. *FEBS Lett.* **582**, 603–610 (2008).

93. Bono, F. & Fiorentini, C. Exploring pre-degenerative alterations in humans using induced pluripotent stem cell-derived dopaminergic neurons. *Neural Regeneration Research* **12**, 1068–1070 (2017).

94. Shaerzadeh, F. *et al.* Microglia senescence occurs in both substantia nigra and ventral tegmental area. *Glia* (2020). doi:10.1002/glia.23834

95. Shioda, N. *et al.* Endocytosis following dopamine D2 receptor activation is critical for neuronal activity and dendritic spine formation via Rabex-5/PDGFRβ signaling in striatopallidal medium spiny neurons. *Mol. Psychiatry* **22**, 1205–1222 (2017).

96. SHOLL, D. A. Dendritic organization in the neurons of the visual and motor cortices of the cat. *J. Anat.* **87**, 387–406 (1953).

97. Benavides-Piccione, R., Hamzei-Sichani, F., Ballesteros-Yáñez, I., Defelipe, J. & Yuste, R. Dendritic size of pyramidal neurons differs among mouse cortical regions. *Cereb. Cortex* **16**, 990–1001 (2006).

98. O'Neill, K. M. *et al.* Assessing effects on dendritic arborization using novel Sholl analyses. *Front. Cell. Neurosci.* **9**, 285 (2015).

99. Levy, M., Lu, Z., Dion, G. & Kara, P. The shape of dendritic arbors in different functional domains of the cortical orientation map. *J. Neurosci.* **34**, 3231–3236 (2014).

100. Brown, K. M., Gillette, T. A. & Ascoli, G. A. Quantifying neuronal size: Summing up trees and splitting the branch difference. *Seminars in Cell and Developmental Biology* **19**, 485–493 (2008).

101. Ballion, B. *et al.* D2 receptor stimulation, but not D1, restores striatal equilibrium in a rat model of Parkinsonism. *Neurobiol. Dis.* **35**, 376–384 (2009).

102. Kihara, T. *et al.* Protective effect of dopamine D2 agonists in cortical neurons via the phosphatidylinositol 3 kinase cascade. *J. Neurosci. Res.* **70**, 274–282 (2002).

103. Hill, M. P. *et al.* Antiparkinsonian effects of the novel D3/D2 dopamine receptor agonist, S32504, in MPTP-lesioned marmosets: Mediation by D2, not D3, dopamine receptors. *Mov. Disord.* **21**, 2090–2095 (2006).

104. Wiemerslage, L., Schultz, B. J., Ganguly, A. & Lee, D. Selective degeneration of dopaminergic neurons by MPP^+ and its rescue by D2 autoreceptors in *Drosophila* primary culture. *J. Neurochem.* **126**, 529–540 (2013).

105. O'Malley, K. L. The Role of Axonopathy in Parkinson's Disease. *Exp. Neurobiol.* **19**, 115–119 (2010).

106. Tagliaferro, P. & Burke, R. E. Retrograde Axonal Degeneration in Parkinson Disease. *Journal of Parkinson's Disease* **6**, 1–15 (2016).

107. Du, F., Li, R., Huang, Y., Li, X. & Le, W. Dopamine D3 receptor-preferring agonists induce neurotrophic effects on mesencephalic dopamine neurons. *Eur. J. Neurosci.* **22**, 2422–2430 (2005).

108. Bono, F. *et al.* Role of Dopamine D2/D3 Receptors in Development, Plasticity, and Neuroprotection in Human iPSC-Derived Midbrain Dopaminergic Neurons. *Mol. Neurobiol.* **55**, 1054–1067 (2018).

109. Koller, W., Herbster, G., Anderson, D., Wack, R. & Gordon, J. Quinpirole hydrochloride, a potential anti-parkinsonism drug. *Neuropharmacology* **26**, 1031–1036 (1987).

110. Swarzenski, B. C., Tangt, L., Oht, Y. J., O'malleyt, K. L. & Todd, R. D. *Morphogenic potentials of D2, D3, and D4 dopamine receptors revealed in transfected neuronal cell lines (neuronal development/mesencephalic cells)*. **91**, (1994).

111. Sung, Y. K. *et al.* The dopamine D2 receptor regulates the development of dopaminergic neurons via extracellular signal-regulated kinase and Nurr1 activation. *J. Neurosci.* **26**, 4567–4576 (2006).

112. Vergara, R. C. *et al.* The Energy Homeostasis Principle: Neuronal Energy Regulation Drives Local Network Dynamics Generating Behavior. *Front. Comput. Neurosci.* **13**, (2019).

113. Pissadaki, E. K. & Bolam, J. P. The energy cost of action potential propagation in dopamine neurons: clues to susceptibility in Parkinson's disease. *Front. Comput. Neurosci.* **7**, 13 (2013).

114. Meiser, J., Weindl, D. & Hiller, K. Complexity of dopamine metabolism. *Cell Commun. Signal.* **11**, 34 (2013).

115. Delcambre, S., Nonnenmacher, Y. & Hiller, K. Dopamine metabolism and reactive oxygen species production. in *Mitochondrial Mechanisms of Degeneration and Repair in Parkinson's Disease* 25–47 (Springer International Publishing, 2016). doi:10.1007/978-3-319-42139-1_2

116. Burke, W. J., Li, S. W., Williams, E. A., Nonneman, R. & Zahm, D. S. 3,4-Dihydroxyphenylacetaldehyde is the toxic dopamine metabolite in vivo: Implications for Parkinson's disease pathogenesis. *Brain Res.* **989**, 205–213 (2003).

117. Hastings, T. G. Enzymatic Oxidation of Dopamine: The Role of Prostaglandin H Synthase. *J. Neurochem.* **64**, 919–924 (1995).

118. Spencer, J. P. E. *et al.* Conjugates of Catecholamines with Cysteine and GSH in Parkinson's Disease: Possible Mechanisms of Formation Involving Reactive Oxygen Species. *J. Neurochem.* **71**, 2112–2122 (2002).

119. Mattammal, M. B., Haring, J. H., Chung, H. D., Raghu, G. & Strong, R. An endogenous dopaminergic neurotoxin: Implication for Parkinson's disease. *Neurodegeneration* **4**, 271–281 (1995).

120. Hastings, T. G., Lewis, D. A. & Zigmond, M. J. Role of oxidation in the neurotoxic effects of intrastriatal dopamine injections. *Proc. Natl. Acad. Sci. U. S. A.* **93**, 1956–1961 (1996).

121. Roy, S. Synuclein and dopamine: The Bonnie and Clyde of Parkinson's disease. *Nature Neuroscience* **20**, 1514–1515 (2017).

122. Escobar, A. P. *et al.* Reduced dopamine and glutamate neurotransmission in the nucleus accumbens of quinpirole-sensitized rats hints at inhibitory D2 autoreceptor function. *J. Neurochem.* **134**, 1081–1090 (2015).

123. Mishra, A., Singh, S. & Shukla, S. Physiological and Functional Basis of Dopamine Receptors and Their Role in Neurogenesis: Possible Implication for Parkinson's disease. *Journal of Experimental Neuroscience* **12**, (2018).

124. Pothos, E. N., Przedborski, S., Davila, V., Schmitz, Y. & Sulzer, D. D2-like dopamine autoreceptor activation reduces quantal size in PC 12 cells. *J. Neurosci.* **18**, 5575–5585 (1998).

125. Bull, D. R., Bakhtiar, R. & Sheehan, M. J. Characterization of dopamine autoreceptors in the amygdala: A fast cyclic voltammetric study in vitro. *Neurosci. Lett.* **134**, 41–44 (1991).

126. Hadjiconstantinou, M., Neff, N. H., Zhou, L. W. & Weiss, B. D2 dopamine receptor antisense increases the activity and mRNA of tyrosine hydroxylase and aromatic L-amino acid decarboxylase in mouse brain. *Neurosci. Lett.* **217**, 105–108 (1996).

127. Sibley, D. R. NEW INSIGHTS INTO DOPAMINERGIC RECEPTOR FUNCTION USING ANTISENSE AND GENETICALLY ALTERED ANIMALS. *Annu. Rev. Pharmacol. Toxicol.* **39**, 313–341 (1999).

128. Carter, A. J. & Müller, R. E. Pramipexole, a dopamine D2 autoreceptor agonist, decreases the extracellular concentration of dopamine in vivo. *Eur. J. Pharmacol.* **200**, 65–72 (1991).

129. Schapira, A. H. V. & Olanow, C. W. Rationale for the use of dopamine agonists as neuroprotective agents in Parkinson's disease. *Ann. Neurol.* **53**, S149–S159 (2003).

130. Sang, K. P. *et al.* Par-4 links dopamine signaling and depression. *Cell* **122**, 275–287 (2005).

131. Parvez, S., Winkler-Stuck, K., Hertel, S., Schönfeld, P. & Siemen, D. The dopamine-D2-receptor agonist ropinirole dose-dependently blocks the Ca2+-triggered permeability transition of mitochondria. *Biochim. Biophys. Acta - Bioenerg.* **1797**, 1245–1250 (2010).

132. Benoit-Marand, M., Borrelli, E. & Gonon, F. Inhibition of dopamine release via presynaptic D2 receptors: Time course and functional characteristics in vivo. *J. Neurosci.* **21**, 9134–9141 (2001).

133. Oh, M. S., Hong, S. J., Huh, Y. & Kim, K. S. Expression of transgenes in midbrain dopamine neurons using the tyrosine hydroxylase promoter. *Gene Ther.* **16**, 437–440 (2009).

134. Chakrabarty, P. *et al.* Capsid Serotype and Timing of Injection Determines AAV Transduction in the Neonatal Mice Brain. *PLoS One* **8**, (2013).

135. Sun, F. *et al.* A Genetically Encoded Fluorescent Sensor Enables Rapid and Specific Detection of Dopamine in Flies, Fish, and Mice. *Cell* **174**, 481-496.e19 (2018).

136. Sorrentino, Z. A. *et al.* Physiological C-terminal truncation of α-synuclein potentiates the prion-like formation of pathological inclusions. *J. Biol. Chem.* **293**, 18914–18932 (2018).

137. Dhillon, J.-K. S. *et al.* A novel panel of α-synuclein antibodies reveal distinctive staining profiles in synucleinopathies. *PLoS One* **12**, e0184731 (2017).

138. Vickery, R. G. & Von Zastrow, M. Distinct dynamin-dependent and -independent mechanisms target structurally homologous dopamine receptors to different endocytic membranes. *J. Cell Biol.* **144**, 31–43 (1999).

139. Kabbani, N., Negyessy, L., Lin, R., Goldman-Rakic, P. & Levenson, R. Interaction with neuronal calcium sensor NCS-1 mediates desensitization of the D2 dopamine receptor. *J. Neurosci.* **22**, 8476–8486 (2002).

140. Jensen, K. L., Runegaard, A. H., Weikop, P., Gether, U. & Rickhag, M. Assessment of dopaminergic homeostasis in mice by use of highperformance liquid chromatography analysis and synaptosomal dopamine uptake. *J. Vis. Exp.* **2017**, 56093 (2017).

141. Mauna, J. C. *et al.* G protein βγ subunits play a critical role in the actions of amphetamine. *Transl. Psychiatry* **9**, 1–11 (2019).

142. Koutzoumis, D. N. *et al.* Alterations of the gut microbiota with antibiotics protects dopamine neuron loss and improve motor deficits in a pharmacological rodent model of Parkinson's disease. *Exp. Neurol.* **325**, 113159 (2020).

143. Heindl, S. *et al.* Automated morphological analysis of microglia after stroke. *Front. Cell. Neurosci.* **12**, (2018).

144. Xu, H. *et al.* Environmental enrichment potently prevents microglia-mediated neuroinflammation by human amyloid β-protein oligomers. *J. Neurosci.* **36**, 9041–9056 (2016).

Figure Legends:

Figure 1. Tyrosine hydroxylase (TH) promoter driven adeno-associated virus (AAV) efficiently transduces human α-synuclein or the control construct (TH-GFP) in midbrain dopamine neurons. (A, B) Immunolabeling of TH confirmed 91% ± 3 of TH positive neurons co-express GFP, suggesting a high fidelity for pAAV1-TH-GFP viral transduction in the TH positive neurons (n = 3 independent experiments). (C, D) The transduction of pAAV1-TH-human-αsyn in midbrain dopaminergic neurons was confirmed via immunocytochemistry analysis and western blot (n = 4 independent experiments, see supplemental figure 1 for Western blot analysis). Scale bars: 50 μm.

Figure 2. Overexpression of α-synuclein disrupts calcium dynamics and firing activity of dopaminergic neurons. (A) Top – Representative spontaneous GCaMP6f calcium activity in naive dopaminergic neurons (left, black) and dopaminergic neurons overexpressing α-syn (right, pink) exemplify the alteration in calcium dynamics due to increased levels of α-syn. Bottom – Spontaneous calcium activity encompassing all neurons recorded in each experimental group (n = 33 wild type neurons, n = 40 α-syn overexpressing neurons, form 8 biological replicates). (B) Calcium events in all neurons were defined as fluctuations of the fluorescent signal at least two standard deviations above the fluorescence baseline value. (C) Spontaneous calcium events were quantified for event rate, width, and amplitude. Whereas overexpression of α-syn does not alter calcium event rate ($p = 0.2596$, one-way ANOVA, $F(2,65) = 1.38$ n = 33 wild type neurons, n = 40 α-syn overexpressing neurons), α-syn burden results in broadening of calcium events ($p = 0.034$, one-way ANOVA, $F(2,97) = 3.89$, n = 33 wild type neurons, n = 40 α-syn overexpressing neurons) and increases in amplitude ($p = 0.000002$, one-way ANOVA, $F(2,1294) = 12.62$, n = 33 wild type neurons, n = 40 α-syn overexpressing neurons). (D) Representative whole cell current-clamp recordings of spontaneously active naive (left, black) dopaminergic neuron compared with a dopaminergic neuron overexpressing α-syn (right, pink). (E) Naïve dopaminergic neurons fire in a canonical pacemaker pattern and consistent rate, whereas with α-syn overexpressing they fire significantly more frequently (firing frequency: from eight independent experiments, 1.132 ± SEM for naive neurons vs. 3.187 ± SEM for α-syn overexpressing neurons, two-tailed unpaired t-test, $p = 0.0142$; interspike interval (ISI): 1143 ± SEM for naive neurons compared to 497.9 ± SEM for α-syn overexpressing neurons, two-tailed unpaired t-test, $p = 0.0431$) and trend in bursts with intermediated periods of quiescence (CV of ISI – 1.676 ± SEM for naive neurons vs. 2.932 for α-syn overexpressing neurons, two-tailed unpaired t-test, $p = 0.0808$ box plot whiskers represent the 95% confidence interval, the upper and lower bounds of the box represent the 75^{th} and 25^{th} percentiles, respectively, with the middle line indicative of the median value of the sample). Empty circles in panel C represent statistical outliers all of which were included in the analyses. Bar graphs ± SEM are overlaid with individual filled data points.

Figure 3: α-synuclein overexpression reduces D2 receptor autoinhibition.
Live-cell GCaMP6f calcium imaging in DAT-cre-GCaMP6f-expressing dopamine neurons was employed to measure the peak amplitude of calcium events at baseline (sampling frequency of 1 image/second), and after bath application of dopamine (1 μM) or quinpirole

(10 μM) for 150 seconds (sampling frequency of 1 image/second). Peak fluorescence intensities were normalized to average baseline GCaMP6f fluorescence intensity (initial 60 seconds). The dotted line denotes normalized average baseline GCaMP6f fluorescence intensity (30 seconds prior to treatment shown). (A) Top panels – representative images of naive dopaminergic neurons and bottom panels – α-syn overexpressing dopaminergic neurons before (left panel) and during dopamine (1 μM) administration (right panels). (B) Top – In naive dopaminergic neurons, bath application of dopamine rapidly and significantly reduced the GCaMP6f fluorescence intensity (n = 14-21, two-way ANOVA where the variables are time and treatment followed by Tukey's HSD, p = 0.0003, from five independent replicates). Bottom – In α-syn overexpressing dopaminergic neurons, bath application of dopamine produced a smaller reduction in the peak amplitude of calcium events as indicated by decreased GCaMP6f fluorescence intensity (n = 17-26, two-way ANOVA where the variables are time and treatment followed by Tukey's HSD, p = 0.0088, from five independent replicates). (C) The fold change in the average GCaMP6f fluorescence intensity before and after drug administration. Dopamine-mediated autoinhibition response is reduced in α-syn overexpressing neurons (n = 11-17, one-way ANOVA followed by Tukey's HSD, naive vs. α-synuclein overexpression, p = 0.0035, naive vs. GFP p = 0.2927 and α-syn vs. GFP p = 0.0001, from five independent replicates). (D) Representative images of naive dopaminergic neurons (top panels) and α-syn overexpressing dopaminergic neurons (bottom panels), before (left panels) and after quinpirole (10 μM) administration (right panels). (E) In naive dopaminergic neurons, bath application of quinpirole rapidly and significantly reduced the GCaMP6f fluorescence intensity (top panel) (n = 11-21, two-way ANOVA where the variables are time and treatment, p = 0.0007, from five independent biological replicates). In α-syn overexpressing neurons, bath application of quinpirole produced a smaller reduction in the peak amplitude of calcium events, as indicated by a smaller decrease in GCaMP6f fluorescence intensity (bottom panel) (n = 13-26, two-way ANOVA where the variables are time and treatment, p = 0.7259, from five independent replicates). (F) Fold change in GCaMP6f fluorescence intensity before and after drug administration (n = 11-13, one-way ANOVA followed by Tukey's HSD, naive vs. α-syn overexpression, p = 0.0318, naive vs. GFP p = 0.8178, and α-syn vs. GFP p = 0.0057, from five independent replicates). (G) Left – A representative recording of the spontaneous firing activity of naive dopaminergic neurons before and during quinpirole (10 μM) administration exhibiting the characteristic decrease in firing activity during bath application of drug (n = 6, from three independent biological replicates). Right – A representative recording of the spontaneous firing activity of α-syn overexpressing dopaminergic neurons before and during quinpirole (10 μM) administration showing delayed and reduced reduction in firing activity (n = 8, from three independent experiments). (H) Comparison of the firing frequency of naive (black bar) and α-syn overexpressing neurons (pink bar) during quinpirole administration. The α-syn overexpressing neurons show a delayed and reduced response to quinpirole-inhibition of firing activity (n = 7 from independent experiments, 0.1812 ± SEM for naive neurons vs. 0.7930 ± SEM for α-syn treated with quinpirole, two-tailed unpaired t-test, p = 0.0356), with (I) similar interspike intervals (n = 7 from independent experiments, 11,118 ± SEM for naive neurons vs. 3786 ± SEM for α-syn neurons treated with quinpirole, two-tailed unpaired t-test, p = 0.1197) and (J) firing regularity (CV of ISI – n = 7 from independent experiments, 2.06 ± SEM for naive neurons vs. 1.659 ± SEM for α-syn

neurons treated with quinpirole, two-tailed t-test, p = 0.4507). The data shown in this figure are presented as mean ± SEM overlaid with data points.

Figure 4: Overexpression of α-synuclein increases intra- and extracellular dopamine levels with concurrent increased tyrosine hydroxylase expression.
(A) Schematic and representative baseline-subtracted images of $GRAB_{DA4.4}$-expressing HEK293 ($GRAB_{DA4.4}$-HEK) cells exposed to increasing concentration of dopamine in the imaging solution. Scale bar = 20 μm. (B) A standard curve was generated by plotting the fluorescence intensity of $GRAB_{DA4.4}$-HEK cells against known extracellular dopamine concentrations (R^2=0.98). (C) Constitutive $GRAB_{DA4.4}$-HEK cell fluorescence signal in absence of dopamine neurons (in culture) was obtained at the beginning of each experiment, where the cells were plated in similar conditions sans neurons (F_c). Scale bar = 10 μm. (D) Schematic of experimental procedure where $GRAB_{DA4.4}$-HEK cells were seeded into dopaminergic cultures. In the presence of dopamine, $GRAB_{DA4.4}$-HEK cells rapidly increase in fluorescence intensity. $GRAB_{DA4.4}$-HEK cells were co-cultured for 20-24 hours with DATCre-GCaMP6f midbrain dopamine neurons prior to experimentation. Viral transduction of floxed tdTomato (red) enabled isolation of the GCaMP6f signal from $GRAB_{DA4.4}$ signal. (E) Baseline fluorescence levels denote the basal, unstimulated, and spontaneous dopamine release from the neurons. To compare baseline dopamine release amongst the experimental groups, the average ratio of the fluorescence signal of the cells adjacent to neuron soma and neuronal processes to the average ratio of $GRAB_{DA4.4}$-HEK cells (only) were calculated (Relative Fluorescence = (F $GRAB_{DA4.4}$-HEK cells grown with neurons - F_c) /F_c). To compare KCl-stimulated dopamine release, the changes on the average fluorescence signal of cells adjacent to the neuron soma and neuronal processes before and after KCl were calculated (Relative Fluorescence = ($F_{stimulated} - F_{baseline}$) /$F_{baseline}$). $GRAB_{DA4.4}$-HEK cells co-cultured with α-syn overexpressing neurons show significantly higher basal extracellular dopamine release (relative fluorescence) compared to naive and AAV-TH-GFP expressing neurons. Scale bar = 50 μm. (F) Bar graph shows $GRAB_{DA4.4}$-HEK cells co-cultured with α-syn overexpressing neurons show higher basal fluorescence, indicating higher baseline dopamine release (n = 10 from three independent replicates; the data are means ± S.E.M., one-way ANOVA followed by Tukey's HSD, F(2,167) = 13.05, naive vs. α-syn p = 0.0007, naive vs. GFP p = 0.9866 and GFP vs. α-syn p = 0.0001). (G) Bath application of 90 mM KCl (positive control for maximal dopamine release) reveals similar relative fluorescence responses across groups, indicating similar maximal dopamine release (n = 10 from three independent replicates; the data are mean ± S.E.M. analyzed by one-way ANOVA followed by Tukey's HSD, F(2,68) = 0.2540, naive vs. α-syn p = 0.9872, naive vs. GFP p = 0.8651 and GFP vs. α-syn p = 0.7827). (H, I) To further directly measure intra- and extracellular dopamine levels, HPLC analyses was used to complement the $GRAB_{DA4.4}$-HEK results. HPLC quantification of dopamine levels in the in the media (H, extracellular milieu) and cell lysate (I, intracellular milieu) revealed increased intracellular and extracellular dopamine levels in α-syn overexpressing neurons compared to naive and AAV-TH-GFP-expressing neurons (n = 8 each, from 8 independent replicates, one-way ANOVA followed by Tukey's HSD, intracellular : F(3,22) = 9.376, naive vs. α-syn p = 0.0059, naive vs. GFP p = 0.5164 and GFP vs. α-syn p = 0.0003; and extracellular: F(3,22) = 9.525, naive vs. α-syn p = 0.01 , naive vs. GFP p = 0.5235 and GFP vs. α-syn

p = 0.0005). (J) Schematic diagram of quantitative ELISA experimental design for TH in dopaminergic neurons. (K) Standard curve for TH sandwich ELISA shows average absorbance values for each purified TH protein concentration from multiple consecutive experiments (R^2=0.99). (L) TH protein levels were detected and quantified in positive control groups, PC12 cells, whereas, no protein was detected in the negative control group, HEK293 cells. (M) α-Syn overexpressing neurons exhibited increased levels of TH compared to naive and AAV-TH-GFP controls (n = 8-10, one-way ANOVA followed by Tukey's HSD, F(2,23) = 4.488, naive vs. α-syn p = 0.031, naive vs. GFP p = 0.7983, and GFP vs. α-syn p = 0.0491). These experiments were performed through a double-blinded experimental design.

Figure 5: D2 receptor antagonism in dopaminergic neurons mimics burst firing pattern with a significantly higher firing frequency observed in α-synuclein overexpressing dopamine neurons that presents with lower membrane/cytoplasmic D2 ratio. (A-B) Representative whole cell current-clamp recordings of spontaneously active naive (A, black) and α-syn overexpressing (B, pink) dopaminergic neurons during sulpiride (D2 antagonist, 5μM) bath application. (C-E) Bar graph shows firing frequency (C), interspike interval (ISI) (D), and firing regularity (E) during bath application of sulpiride (5μM), revealing D2 antagonism in naive dopaminergic neurons promotes firing rates, interspike intervals, and regularity comparable to neurons overexpressing α-syn (n = 8 from 3 independent biological replicates, two-tailed unpaired t-test, firing frequency: 1.766 ± SEM naive vs. 2.805 ± SEM α-syn overexpressing neurons, p = 0.148, ISI – 1791 ± SEM naive vs. 1221 ± SEM α-syn overexpressing neurons p = 0.1147, CV of ISI - 1.642 naive ± SEM vs. 1.412 ± SEM α-syn overexpressing neurons, p = 0.456). (F-G) Membrane biotinylation experiments. Membrane and cytoplasmic D2 factions were isolated from a separate set of naive and α-syn overexpressing neurons, prepared identically, via a double blinded experimental design. (F) A-syn overexpressing neurons exhibit an increased trend in levels of cytoplasmic D2 receptor relative to total D2 receptor levels (n = 3 from independent replicates, two-tailed unpaired t-test p = 0.1115). (G) The ratio of average membrane D2R to the average cytoplasmic D2R significantly decreases in α-syn overexpressing neurons (n = 3 from independent replicates, two-tailed unpaired t-test p = 0.0178). The data are presented as mean ± SEM with independent replicate data points overlaid.

Figure 6: α-Synuclein overexpression reduces arborization of dopaminergic neurons and treatment with a D2 receptor agonist partially rescues the detrimental impact of α-synuclein. (A) Schematic image explaining the parameters used in the morphological examination (B-D) Representative binarized images of naive (B), α-syn overexpressing (C), and quinpirole pretreated α-syn overexpressing neurons (D). (E-H) Sholl intersection profiles of untreated naive (E), untreated α-syn-overexpressing (F), and quinpirole pretreated α-syn-overexpressing neurons (G) followed by measurement of area under curve (H). Significantly fewer intersections in α-syn overexpressing neurons were observed compared to naive neurons, indicating a marked reduction in neuronal arborization (Tukey's HSD following one-way ANOVA, naive n = 190, α-synuclein, n = 114, naive vs. α-synuclein, p = 0.0009, from at least three independent replicates). Sholl analyses revealed that 48 hours of quinpirole (0.5 μM) pretreatment induces a partial

restoration of neural arborization complexity (described above) compared to untreated α-syn overexpressing neurons (Tukey's HSD following one-way ANOVA, naive n = 190, α-syn n = 114 and α-syn treated with quinpirole n = 32, naive vs. α-syn p = 0.0009, naive vs. α-syn treated with quinpirole p = 0.5131, and α-syn vs. α-syn treated with quinpirole p = 0.0041, from at least three independent replicates). (I) Somatic areas were found to be comparable between experimental groups (Tukey's HSD following one-way ANOVA, naive n = 190, α-syn n = 114, naive vs. α-syn p = 0.67, from at least three independent biological replicates). (J) α-Syn overexpressing dopaminergic neurons project over a much smaller area than naive neurons (Tukey's HSD following one-way ANOVA, naive n = 190, α-syn n = 114, naive vs. α-syn p = 0.0001, from at least three independent biological replicates). (K-M) Morphological measures show detrimental morphological changes in α-syn overexpressing neurons compared to naive control neurons (Tukey's HSD following one-way ANOVA, naive n = 190, α-syn n = 114, circularity: naive vs. α-syn p = 0.0021, outer perimeter: naive vs. α-syn p = 0.0001; width: naive vs. α-syn p = 0.0001, from at least three independent replicates). (K) Circularity of the neurons was measured as ratio of projection area and the projection perimeter ($(4\cdot\pi\cdot\text{area})/\text{perimeter}^2$). (L) Projection field perimeter was defined as the perimeter of the neuronal projection field at the outermost process. (M) Neuronal arborization width was defined as the ratio of projection area to the longest dendritic length of each neuron. D2 receptor agonist partially rescues the detrimental impact of α-synuclein. Quinpirole treatment of α-syn overexpressing neurons rescued changes in (J) projection area (Tukey's HSD following one-way ANOVA, naive n = 190, α-syn n = 114 and α-syn treated with quinpirole n = 32, naive vs. α-syn p = 0.0001, naive vs. α-syn treated with quinpirole p = 0.1136, and α-syn vs. α-syn treated with quinpirole p = 0.0486, from at least three independent replicates), (K) neuronal circularity, (L) projection field perimeter, and (M) arborization width (Tukey's HSD following one-way ANOVA (put in the F(df1,df2) here), naive n = 190, α-syn n = 114, and α-syn treated with quinpirole n = 32, circularity: naive vs. α-syn p = 0.0021, naive vs. α-syn treated with quinpirole p = 0.4452, and α-syn vs. α-syn treated with quinpirole p = 0.0046; outer perimeter: naive vs. α-syn p = 0.0001, naive vs. α-syn treated with quinpirole p = 0.2250, and α-syn vs. α-syn treated with quinpirole p = 0.0312; width: naive vs. α-syn p = 0.0001, naive vs. α-syn treated with quinpirole p = 0.1419, and α-syn vs. α-syn treated with quinpirole p = 0.0187, from at least three independent biological replicates). (N) Dopaminergic neuron counts revealed α-syn overexpression decreases neuronal survival, which is rescued when pretreated with quinpirole (0.5 μM for 48 hours) (Tukey's HSD following one-way ANOVA, naive vs. α-syn p = 0.0008, naive vs. α-syn treated with quinpirole p = 0.1364, and α-syn vs. α-syn treated with quinpirole p = 0.0021, from two independent replicates).

Figure 7: Pretreatment with D2 receptor stimulation partially restores neuronal activity in α-synuclein overexpressing dopamine neurons. (A) To test whether prolonged D2 receptor stimulation ameliorates the impact of α-syn overexpression, dopamine neuronal cultures were incubated with a D2 receptor agonist (quinpirole, 0.5 μM for 48 hours). (B) Spontaneous GCaMP6f calcium activity in a dopaminergic neuron overexpressing α-syn pretreated with quinpirole illustrating a partial restoration of calcium dynamics similar to untreated naive neurons. (C) Calcium events in B were identified as the fluorescent signal increases at least two standard deviations above the fluorescence

baseline value. (D-F) Event rate (D), event width (E), and event amplitude (F) after quinpirole pretreatment. Quinpirole pretreatment reverts the α-syn modulation of calcium homeostasis by preventing the event width broadening, but not the increasing event amplitude or changing the event rates (n = 28 quinpirole treated α-syn overexpressing neurons, two-tailed unpaired t-test, α-syn vs. α-syn pretreated with quinpirole p = 0.2024 event rate, p = 0.0277 event widths, p = 0.6204 event height). Throughout this figure previous data is overlaid with a black dotted line that represents the average values measured for untreated naive neurons and a pink dotted line represents the average values for untreated α-syn overexpressing neurons. Representative of firing activity of an untreated naive neuron (G) and quinpirole pretreated α-syn overexpressing neuron (H). (I-K) Quinpirole treatment partially restores the firing activity of α-syn overexpressing neurons. Quantification of firing frequency (I), interspike interval (J), and firing regularity (K) in quinpirole pretreated α-syn dopamine neuron (n = 7 from three independent biological replicates, 1.325 Hz ± SEM for quinpirole-treated α-syn overexpressing neurons, two-tailed unpaired t-test, α-syn vs. α-syn pretreated with quinpirole p = 0.0342 for firing frequency, p = 0.1053 for ISI, p = 0.4778 for CV of ISI). (L) 20-24 hours prior to experimentation, $GRAB_{DA4.4}$ expressing HEK293 ($GRAB_{DA4.4}$-HEK) cells were seeded at untreated naive (left), untreated α-syn overexpressing (middle) and quinpirole pretreated α-syn overexpressing (right) midbrain neuronal cultures (dopaminergic neurons identified through floxed expression of tdTomato). (M) Quinpirole pretreatment rescued increased dopamine level (quantified as the relative $GRAB_{DA4.4}$ fluorescence levels) in α-syn-overexpressing neurons to level similar to untreated naive neurons (n = 6 from three independent biological replicates; data shown as mean ± SEM, one-way ANOVA followed by Tukey's HSD, naive vs. α-syn treated with quinpirole p = 0.9948, α-syn vs. α-syn treated with quinpirole p = 0.0003) (N,O) $GRAB_{DA4.4}$ signals provide qualitative representation of α-syn-induced dopamine release. Therefore, to corroborate these data, we performed HPLC to quantify intracellular (lysate) and extracellular (media) dopamine levels. The HPLC quantification of dopamine levels revealed that quinpirole pretreatment of α-syn overexpressing neurons reduces both extracellular (N) and intracellular (O) dopamine levels compared to untreated α-syn overexpressing neurons (n = 3 each, from 3 independent biological replicates, one-way ANOVA followed by Tukey's HSD, intracellular: α-syn vs. α-syn treated with quinpirole p = 0.0325 and naive vs. α-syn treated with quinpirole p = 0.9959; extracellular: α-syn vs. α-syn treated with quinpirole p = 0.0449 and naive vs. α-syn treated with quinpirole p = 0.6197). (P) Quantification of TH expression by ELISA. Compared to untreated α-syn overexpressing neurons, quinpirole pretreatment decreased TH protein levels in α-syn overexpressing neurons (n = 3, one-way ANOVA followed by Tukey's HSD, naive vs. α-syn treated with quinpirole p = 0.4288 and α-syn vs. α-syn treated with quinpirole p = 0.6809). The experiments were performed via double-blinded experimental design. Data are presented as mean ± SEM with data points shown.

Supplemental Figure 1: AAV transduction of TH-dependent α-synuclein produces robust overexpression. Quantification of multiple blots illustrating increased α-synuclein levels in naive and transduced cultures (n = 4, two-tailed t-test, p = 0.005).

Supplemental Figure 2: Overexpression of control vector (AAV-TH-GFP) does not affect neural response. (A,B) Neurons overexpressing GFP do not produce responses different from naive neurons in response to either dopamine (A) or quinpirole (B) (Dopamine: n = 11-17, one-way ANOVA followed by Tukey's HSD, naive vs. α-synuclein overexpression, p = 0.0035, naive vs. GFP p = 0.2927 and α-syn vs. GFP p = 0.0001, from five independent replicates, Quinpirole: n = 11-13, one-way ANOVA followed by Tukey's HSD, naive vs. α-syn overexpression, p = 0.0318, naive vs. GFP p = 0.8178, and α-syn vs. GFP p = 0.0057, from five independent replicates).

Table 1:

Primary Neuron Culture

Chemical name	Concentration	Vendor	Catalog Number	Use/ Application	
NaCl	116 mM	Sigma- Aldrich	S7653	dissociation media	
$NaHCO_3$	26 mM	Sigma- Aldrich	S5761	dissociation media	
NaH_2PO_4	2 mM	Sigma- Aldrich	S9638	dissociation media	
D-glucose	25 mM	Sigma- Aldrich	G8769	dissociation media	
$MgSO_4$	1 mM	Sigma- Aldrich	M7506	dissociation media	
Cysteine	1.3 mM	Sigma- Aldrich	C7352	dissociation media	
Papain	400 units/ml	Worthington Biochemical Corporation	LS003127	dissociation media	
Kynurenic acid	0.5 mM	Sigma- Aldrich	K3375	dissociation media	
DMEM	51.45%	Thermo Fisher Scientific	11330032	Glia media	
Fetal Bovine Serum	39.60%	Gemini	100-106	Glia media	
Penicillin/Streptomycin	0.97%	Thermo Fisher Scientific	15-140-122	Glia media	
Glutamax 100X	0.97%	Thermo Fisher Scientific	35050061	Glia media	
Insulin (25mg/ml stock)	0.08%	Sigma-Aldrich	I5500	Glia media	
Neurobasal-A	96.90%	Thermo Fisher Scientific	10888022	DIV0 neuronal media	
B27 Plus	1.90%	Thermo Fisher Scientific	A3582801	DIV0 neuronal media	
GDNF	0.15%	Sigma-Aldrich	SRP3200	DIV0 neuronal media	
Glutamax 100X	0.97%	Thermo Fisher Scientific	35050061	DIV0 neuronal media	
Kynurenic acid	0.08%	Sigma-Aldrich	K3375	DIV0 neuronal media	
Neurobasal-A	97.10%	Thermo Fisher Scientific	10888022	maintenance neuronal media	
B27 Plus	1.90%	Thermo Fisher Scientific	A3582801	maintenance neuronal media	
Glutamax 100X	0.97%	Thermo Fisher Scientific	35050061	maintenance neuronal media	

Live Cell imaging

Chemical name	Concentration	Vendor	Catalog Number	Use/ Application	
NaCl	126 mM	Sigma-Aldrich	S7653	Calcium imaging ACSF	
KCl	2.5 mM	Sigma-Aldrich	P9541	Calcium imaging ACSF	
$CaCl_2$	2 mM	Sigma-Aldrich	223506	Calcium imaging ACSF	
NaH_2PO_4	1.25 mM	Sigma-Aldrich	71505	Calcium imaging ACSF	
$MgSO_4$	2 mM	Sigma-Aldrich	M7506	Calcium imaging ACSF	
Dextrose	10 mM	Sigma-Aldrich	D9434	Calcium imaging ACSF	
$NaHCO_3$	24 mM	Sigma-Aldrich	S5761	Calcium imaging ACSF	
NaCl	92 mM	Sigma-Aldrich	S7653	HEPES ACSF	
KCl	2.5 mM	Sigma-Aldrich	P9541	HEPES ACSF	
$CaCl_2$	0.5 mM	Sigma-Aldrich	223506	HEPES ACSF	
NaH_2PO_4	1.2 mM	Sigma-Aldrich	P5655	HEPES ACSF	
$NaHCO_3$	30 mM	Sigma-Aldrich	S5761	HEPES ACSF	
$MgSO_4$	10 mM	Sigma-Aldrich	M7506	HEPES ACSF	
D-glucose	25 mM	Sigma-Aldrich	G8769	HEPES ACSF	
HEPES	20 mM	Sigma-Aldrich	H3375	HEPES ACSF	
Na-L-ascorbate	5 mM	Sigma-Aldrich	A4034	HEPES ACSF	
Na-pyruvate	3 mM	Sigma-Aldrich	P5280	HEPES ACSF	
Thiourea	2 mM	Sigma-Aldrich	T7875	HEPES ACSF	
Dopamine hydrochloride	1 µM	Sigma-Aldrich	H8502	Treatment	
Quinpirole hydrochloride	10 µM	Sigma-Aldrich	Q102	Treatment	

Electrophysiology

Chemical name	Concentration	Vendor	Catalog Number	Use/ Application	
NaCl	126 mM	Sigma-Aldrich	S7653	Electrophysiology ACSF	
KCl	2.5 mM	Sigma-Aldrich	P9541	Electrophysiology ACSF	
$CaCl_2$	2 mM	Sigma-Aldrich	223506	Electrophysiology ACSF	
NaH_2PO_4	1.25 mM	Sigma-Aldrich	71505	Electrophysiology ACSF	
$MgSO_4$	2 mM	Sigma-Aldrich	M7506	Electrophysiology ACSF	
Dextrose	10 mM	Sigma-Aldrich	D9434	Electrophysiology ACSF	
$NaHCO_3$	26 mM	Sigma-Aldrich	S5761	Electrophysiology ACSF	
Potassium gluconate	120 mM	Sigma-Aldrich	P1847	Electrophysiology ACSF	
$MgCl_2$	2 mM	Sigma-Aldrich	M8266	Electrophysiology ACSF	
HEPES	10 mM	Sigma-Aldrich	H3375	Electrophysiology ACSF	
EGTA	0.1 mM	Sigma-Aldrich	E3889	Electrophysiology ACSF	
$ATPNa_2$	2 mM	Sigma-Aldrich	A2383	Electrophysiology ACSF	
GTPNa	0.25 mM	Sigma-Aldrich	A2383	Electrophysiology ACSF	
Dopamine hydrochloride	1 µM	Sigma-Aldrich	H8502	Electrophysiology ACSF	
Quinpirole hydrochloride	10 µM	Sigma-Aldrich	Q102	Electrophysiology ACSF	

Biochemical Assays

Chemicals	Concentration	Vendor	Catalog Number	Use/ Application	
Phosphate Buffered Saline (PBS)	1X	Prepared as needed on-site	N/A	ICC	
Triton X-100	0.005	Thermo Fisher Scientific	bp151-100	ICC	
Normal Goat Serum (NGS)	0.1	Lampire Biological Products	7332500	ICC	
Paraformaldehyde	0.04	Electron Microscopy Sciences	157-4-100	ICC	
Na_2CO_3	28.3 mM	Sigma-Aldrich	D6546	ELISA Coating Buffer	
$NaHCO_3$	71.42 mM	Sigma-Aldrich	S5761	ELISA Coating Buffer	
Glycerol	10% (v/v)	Sigma-Aldrich	G5516	BufferD Lysis Buffer	
NaCl	125 mM	Sigma-Aldrich	S7653	BufferD Lysis Buffer	
EDTA	1 mM	Sigma-Aldrich	E9884	BufferD Lysis Buffer	
EGTA	1 mM	Sigma-Aldrich	3777	BufferD Lysis Buffer	
NaCl	150 mM	Sigma-Aldrich	S7653	Biotinylation Buffer	
$CaCl_2$	2 mM	Sigma-Aldrich	449709	Biotinylation Buffer	
Triethanolamine	10 mM	Sigma-Aldrich	90279	Biotinylation Buffer	
Sulfo-NHS-SS Biotin	1.5 mg/mL	ThermoFisher Pierce	22331	Biotinylation Buffer	
Monomeric Avidin Resin	n/a	ThermoFisher Pierce	53146	Biotinylation Buffer	
Fat-free milk	1% or 5%	Carnation	N/A	WB/ELISA	
TMB Substrate	Stock	ThermoFisher	34028	ELISA	
H_2SO_4	2N	Sigma-Aldrich	339741	ELISA	
Tween-20	0.002	ThermoFisher	MP1Tween201	WB/ELISA: TBS-T	
Protease Inhibitor	1x	Millipore	539191	WB/ELISA: Cell lysis	
DC Protein assay	N/A	Biorad	5000112	Protein assay	
Immulon 4HBX	N/A	ThermoFisher	3855	ELISA	
NaCl	118 mM	Sigma-Aldrich	S7653	KH Buffer (HPLC)	
KCl	4.7 mM	Sigma-Aldrich	P9541	KH Buffer (HPLC)	
$CaCl_2$	1.25 mM	Sigma-Aldrich	223506	KH Buffer (HPLC)	
KH_2PO_4	1.2 mM	Sigma-Aldrich	P5655	KH Buffer (HPLC)	
$MgSO_4$	1.2 mM	Sigma-Aldrich	M7506	KH Buffer (HPLC)	
D-glucose	11 mM	Sigma-Aldrich	G8769	KH Buffer (HPLC)	

L-Ascorbic acid	0.5 mg/ml	Sigma-Aldrich	A5960	KH Buffer (HPLC)	
$NaHCO_3$	25 mM	Sigma-Aldrich	S5761	KH Buffer (HPLC)	

Antibodies

Primary Antibody	Host Species / isotype	Concentration	Vendor	Catalog Number	Use
Tyrosine Hydroxylase	Rabbit / Polyclonal	1:500	EMD Millipore	AB152	ICC/WB
α-synuclein (syn211)	Mouse/ IgG1	1:500	Abcam	AB80627	ICC
Dopamine Transporter (DAT)	Rat	1:500	Millipore Sigma	AB5802	
Calbindin	Rabbit / Polyclonal	1:500	EMD Millipore	ABN2192	
Green Fluorescent Protein (GFP)	Rabbit / IgG	1:500	ThermoFischer Scientific	A-11122	ICC
Human α-syn (C-terminal regions, 130-140) (94-3A10)	Mouse/ monoclonal IgG1	1:1000	Gifted from Dr. Giasson	N/A	WB
Actin C4	Mouse / Monoclonal	1:1000	EMD Millipore		WB
D2	Mouse	1:1000	Neuromab	75-230	WB/ICC
D2	Rabbit		Millipore		WB
TH	Monoclonal/Mouse	1:1000	EnCor	MCA-4H2	ELISA
TH (Biotin conjugate)	Polyclonal/Rabbit	1:6000	EnCor	RPCA-TH	ELISA
Biotin (HRP conjugate)	N/A (Avidin)	1:200	Vector Labs	A2004	ELISA
Conjugated (or not) Secondary Antibody	**Host species / Target species**	**Concentration**	**Vendor**	**Catalog Number**	**Use**
Alexa Fluor 568	Goat / mouse	1:500	Life Technologies	A-21124	ICC
Alexa Fluor 647	Goat / mouse	1:500	Life Technologies	A-21242	ICC
Alexa Fluor 488	Goat / Rabbit	1:500	Life Technologies	A-11006	ICC
HRP	Goat / Mouse	1:2000	Jackson Immuno Research Labs	AB-10015289	WB
HRP	Goat / Rabbit	1:2000	Jackson Immuno Research Labs	AB_2307391	WB
IRDye® 800CW	Goat / Mouse	1:15000	Li-cor	926-32210	WB

Table 2:

Virus

Viral Vectors (AAV)	Concentration	Vendor	Catalog Number	Capsid Serotype	Other
TH-α-syn	3.26×10^7 units/µl	Dr. Giasson lab	N/A	AAV 1	
TH-GFP	3.26×10^7 units/µl	Dr. Giasson lab	N/A	AAV 1	
LoxP - tdTomato	3.26×10^7 units/µl	Addgene	28306	AAV 1	

Table 2:

Virus

Viral Vectors (AAV)	Concentration	Vendor	Catalog Number	Capsid Serotype	Other
TH-α-syn	3.26×10^{7} units/µl	Dr. Giasson lab	N/A	AAV 1	
TH-GFP	3.26×10^{7} units/µl	Dr. Giasson lab	N/A	AAV 1	
LoxP - tdTomato	3.26×10^{7} units/µl	Addgene	28306	AAV 1	

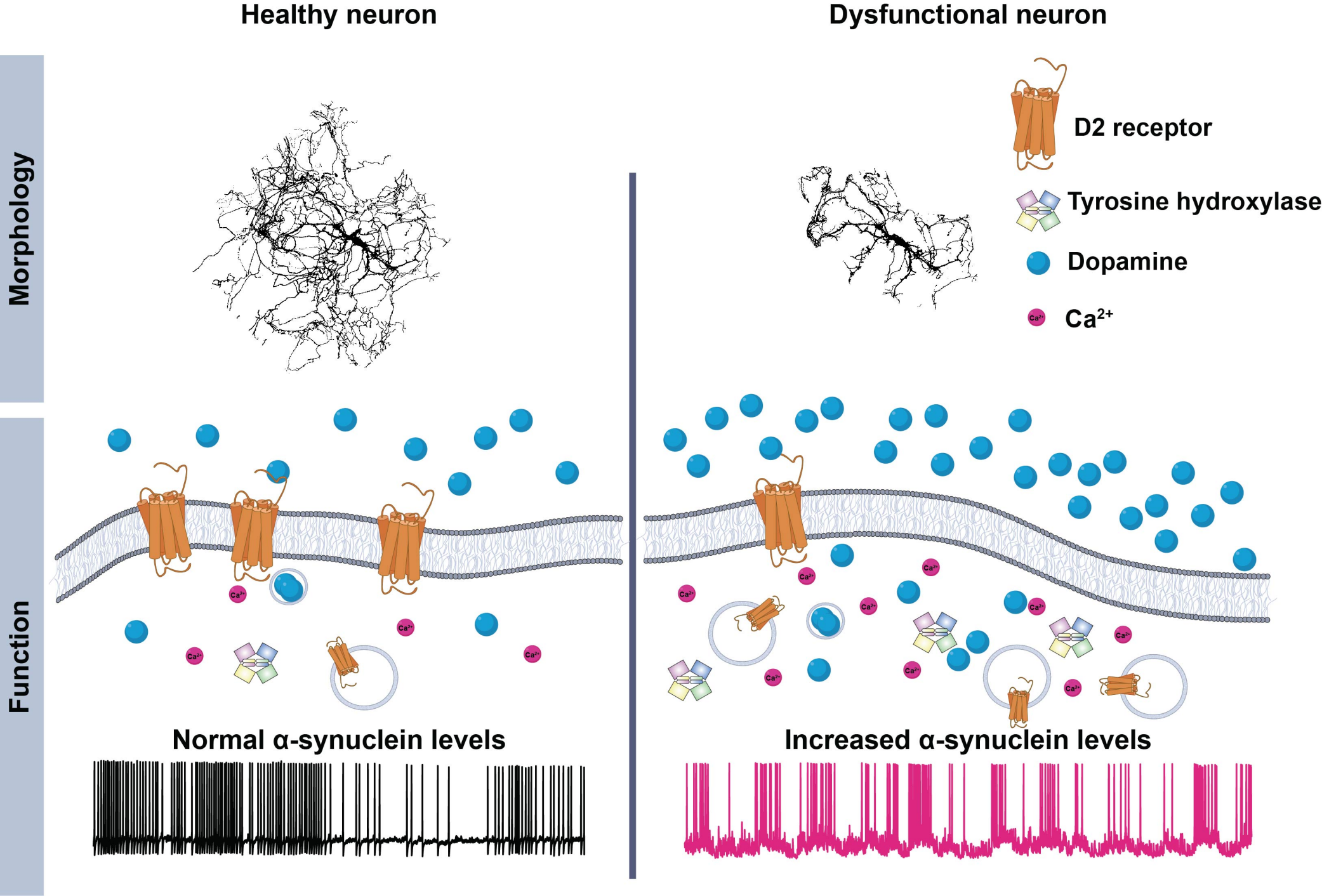
Healthy neuron
Dysfunctional neuron
D2 receptor
Tyrosine hydroxylase
Dopamine
Ca2+
Morphology
Function
Normal α-synuclein levels
Increased α-synuclein levels

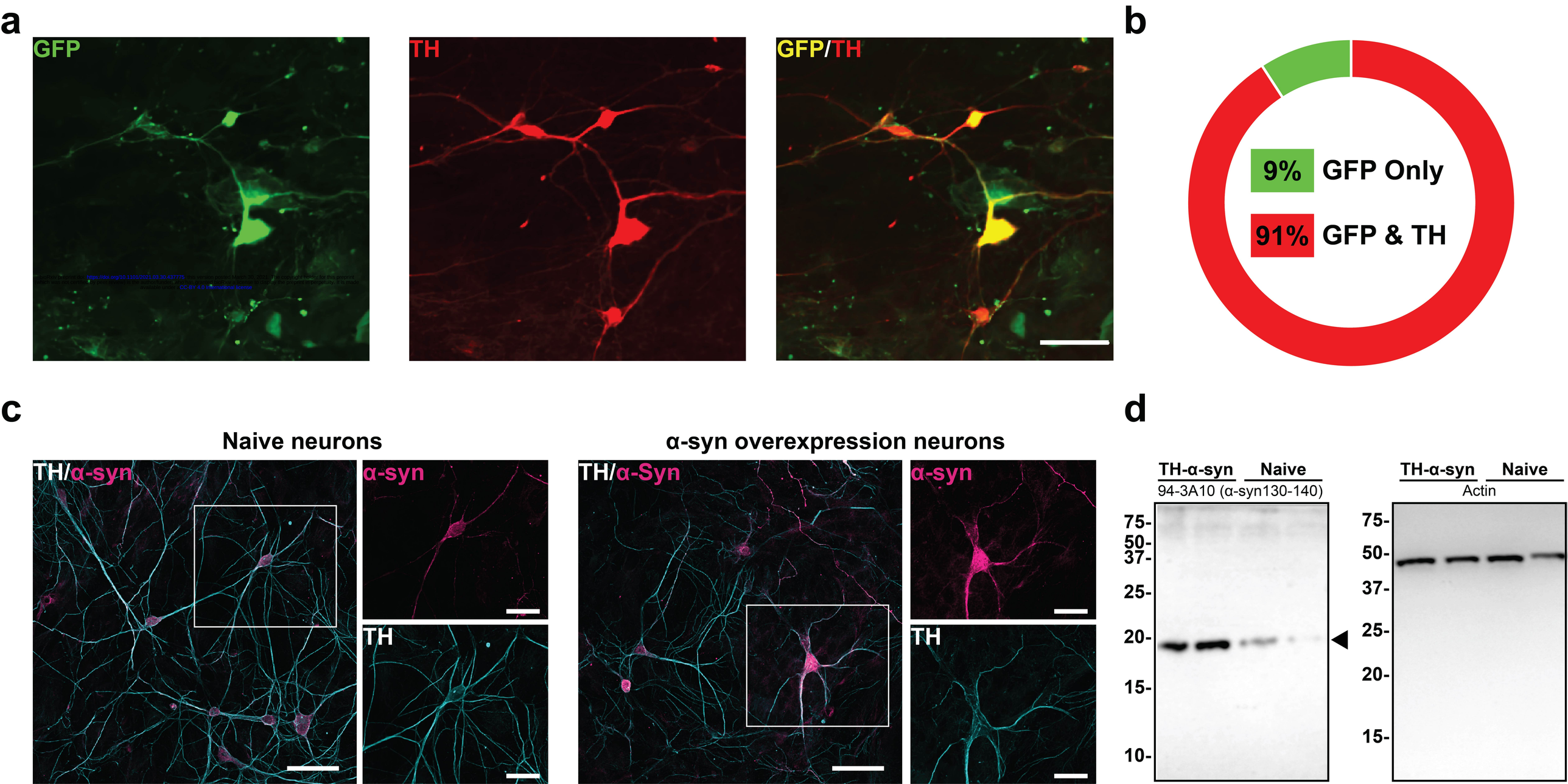

a

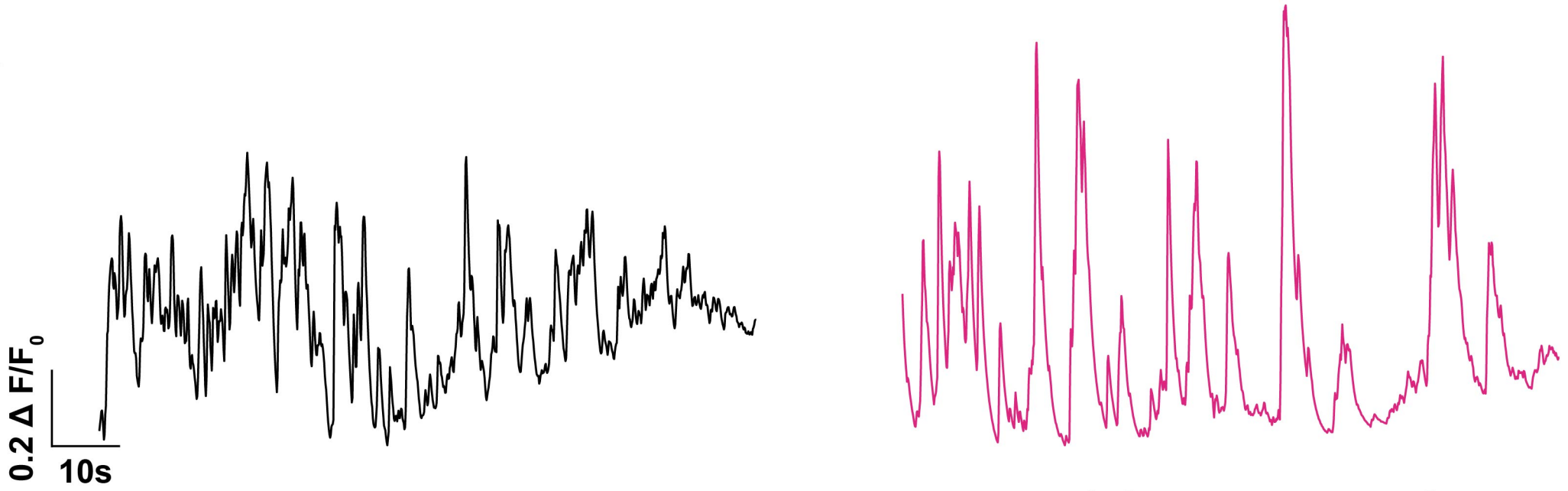

Naive dopamine neuron calcium activity

α-synuclein overexpressing dopamine neuron calcium activity

b

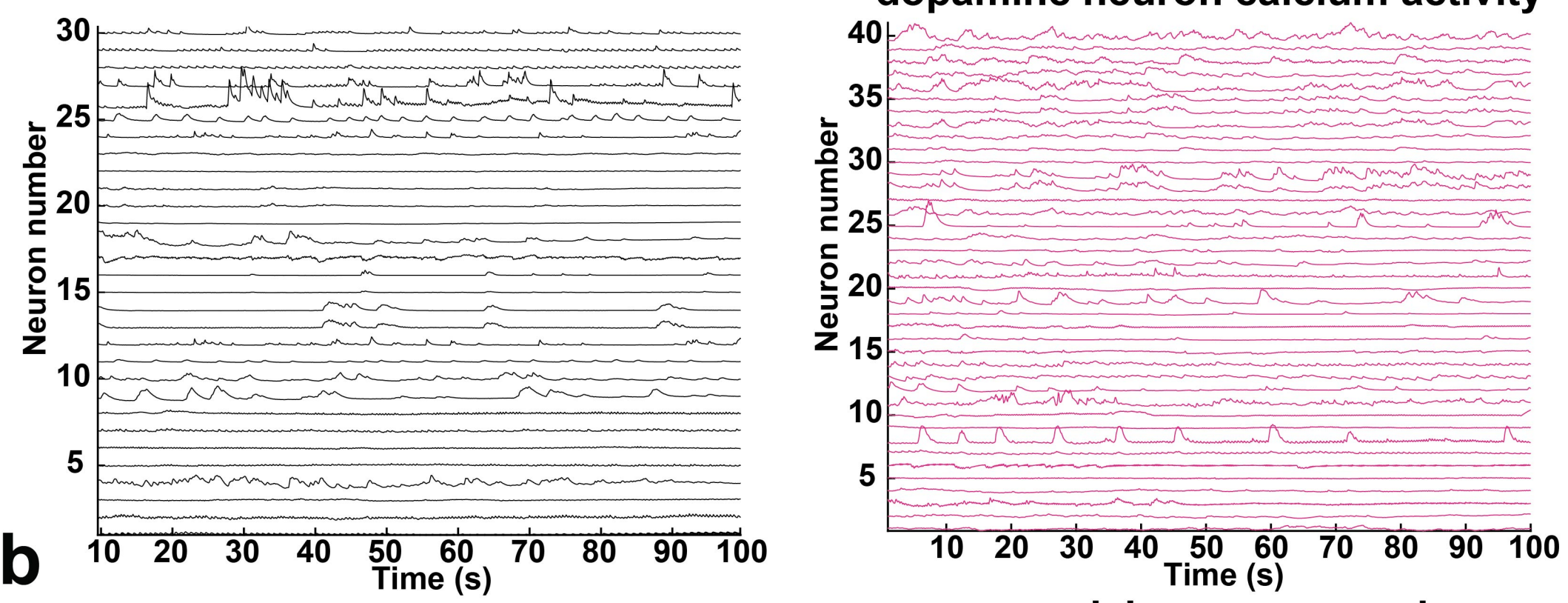

Naive dopamine neuron calcium events

α-synuclein overexpressing dopamine neuron calcium events

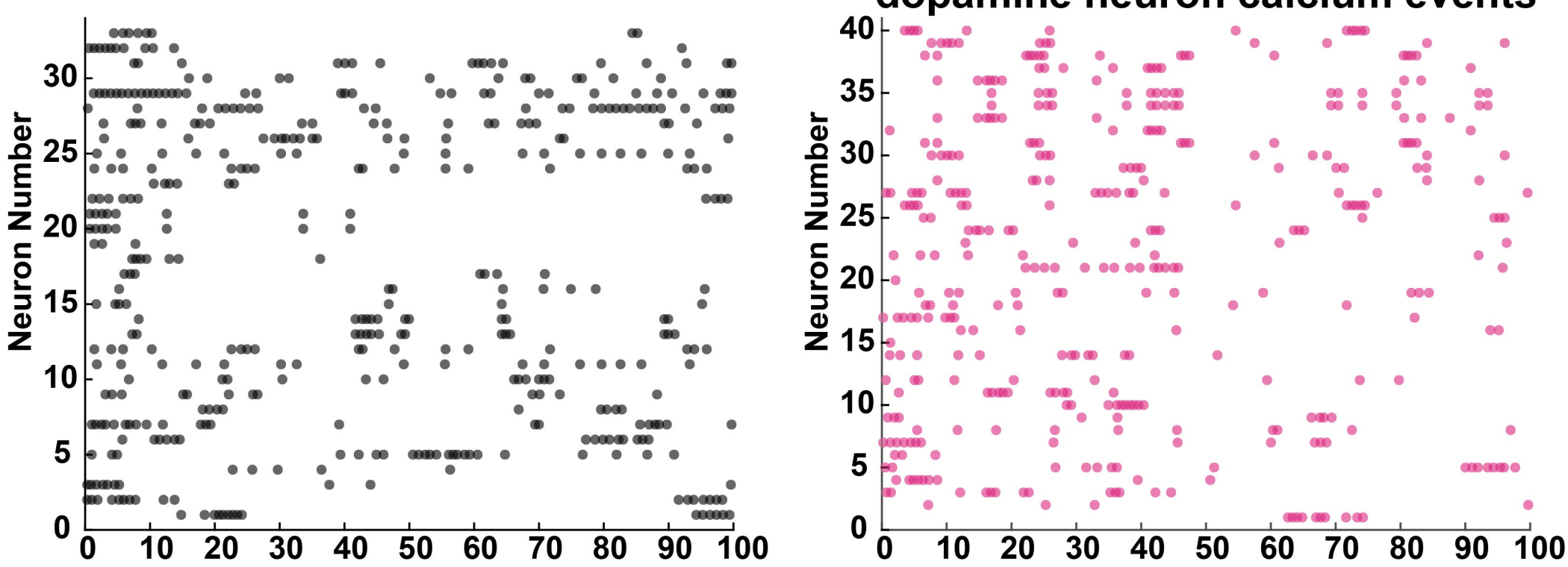

c

Calcium Event Rates

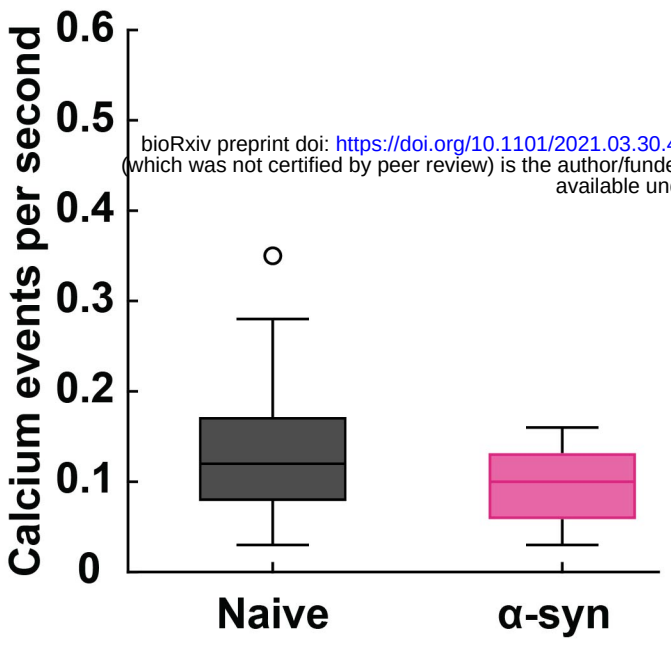

Calcium Event Widths

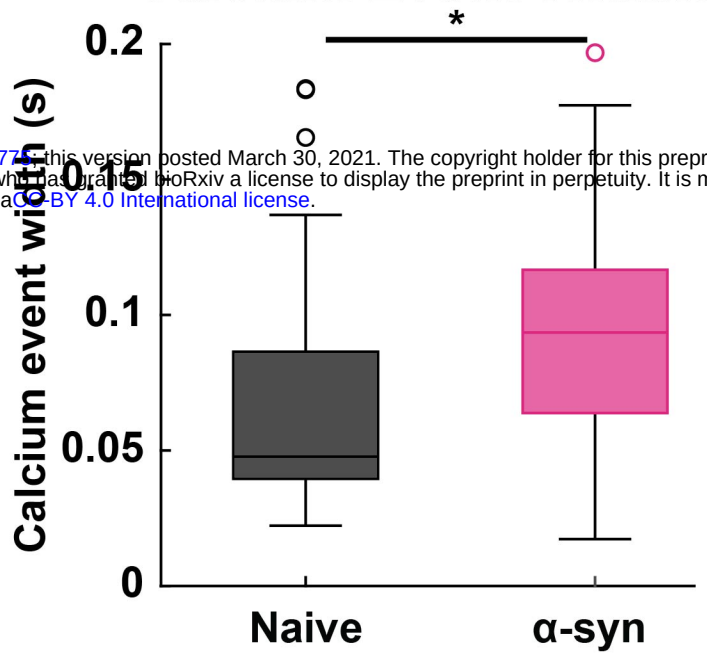

Calcium Event Heights

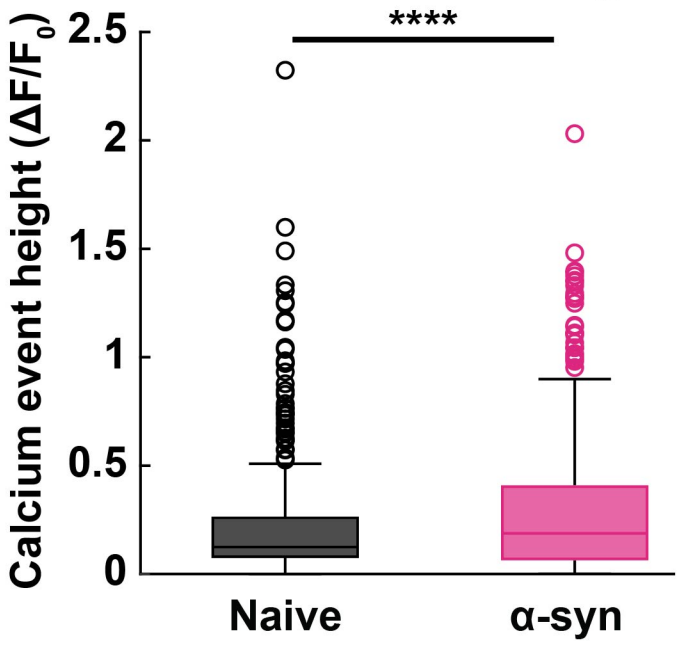

d

Naive spontaneous firing activity

α-synuclein overexpressing spontaneous firing activity

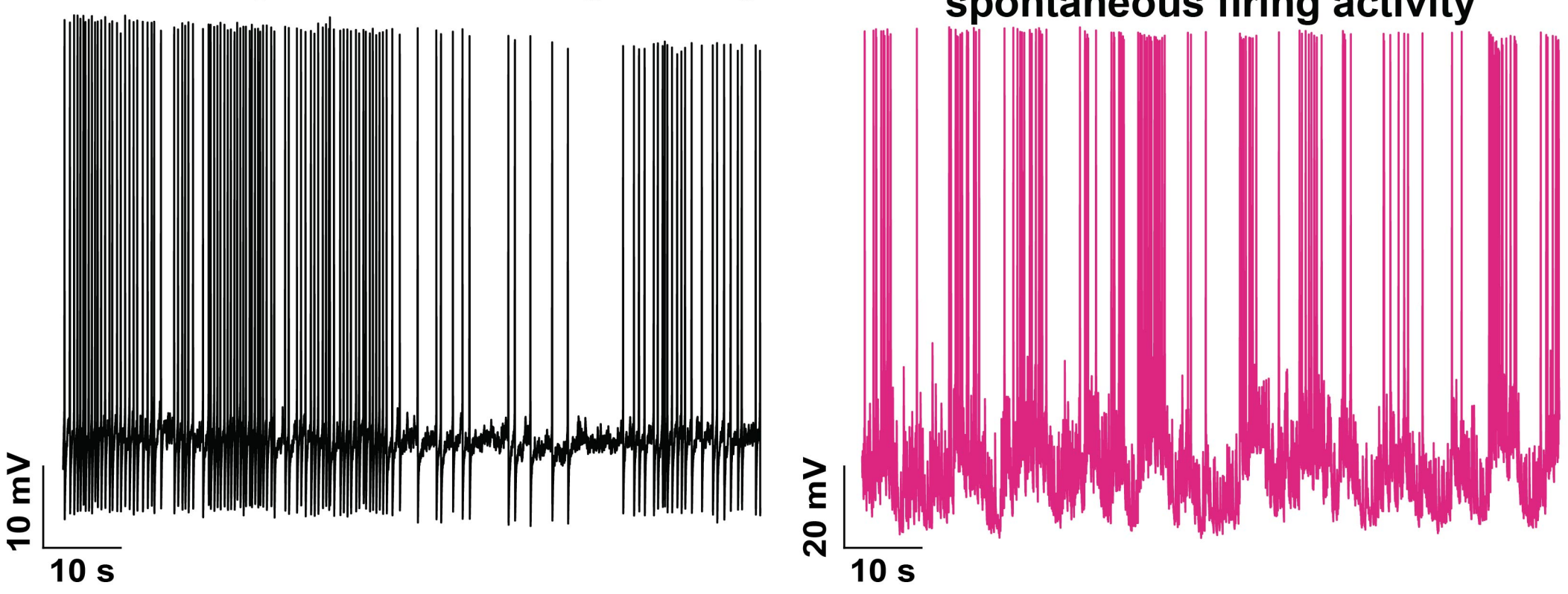

e

Firing Frequency

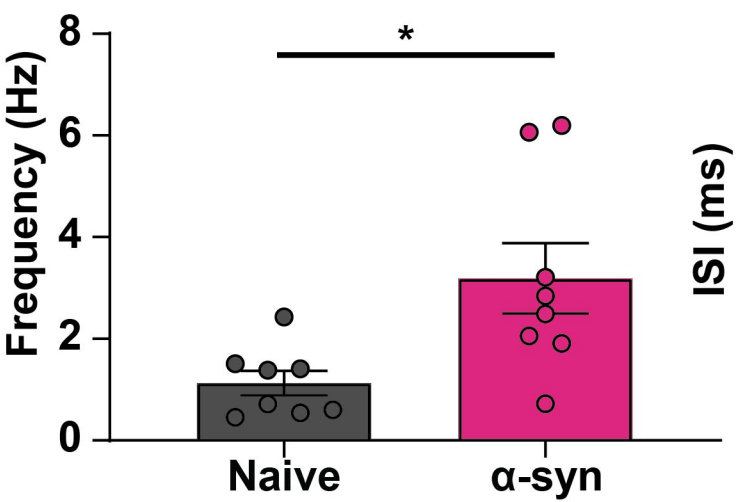

Interspike Interval (ISI)

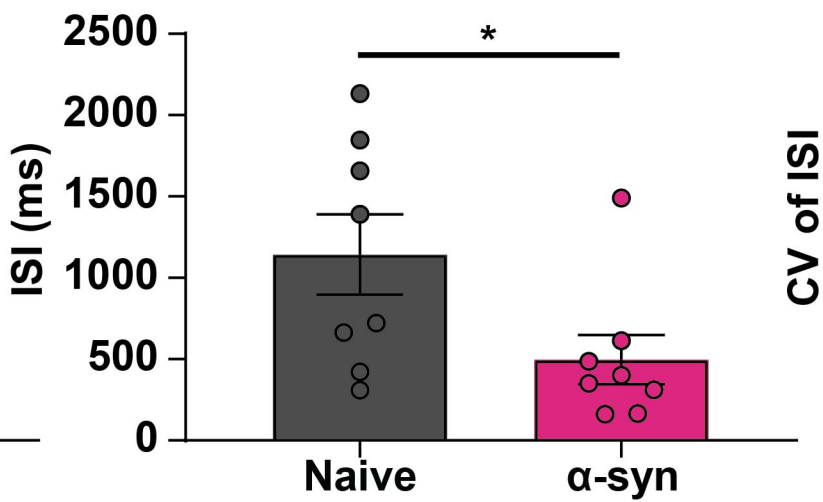

Firing Regularity

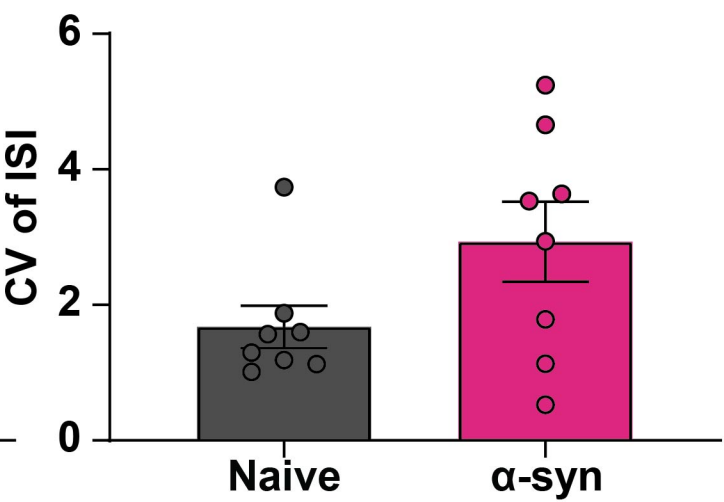

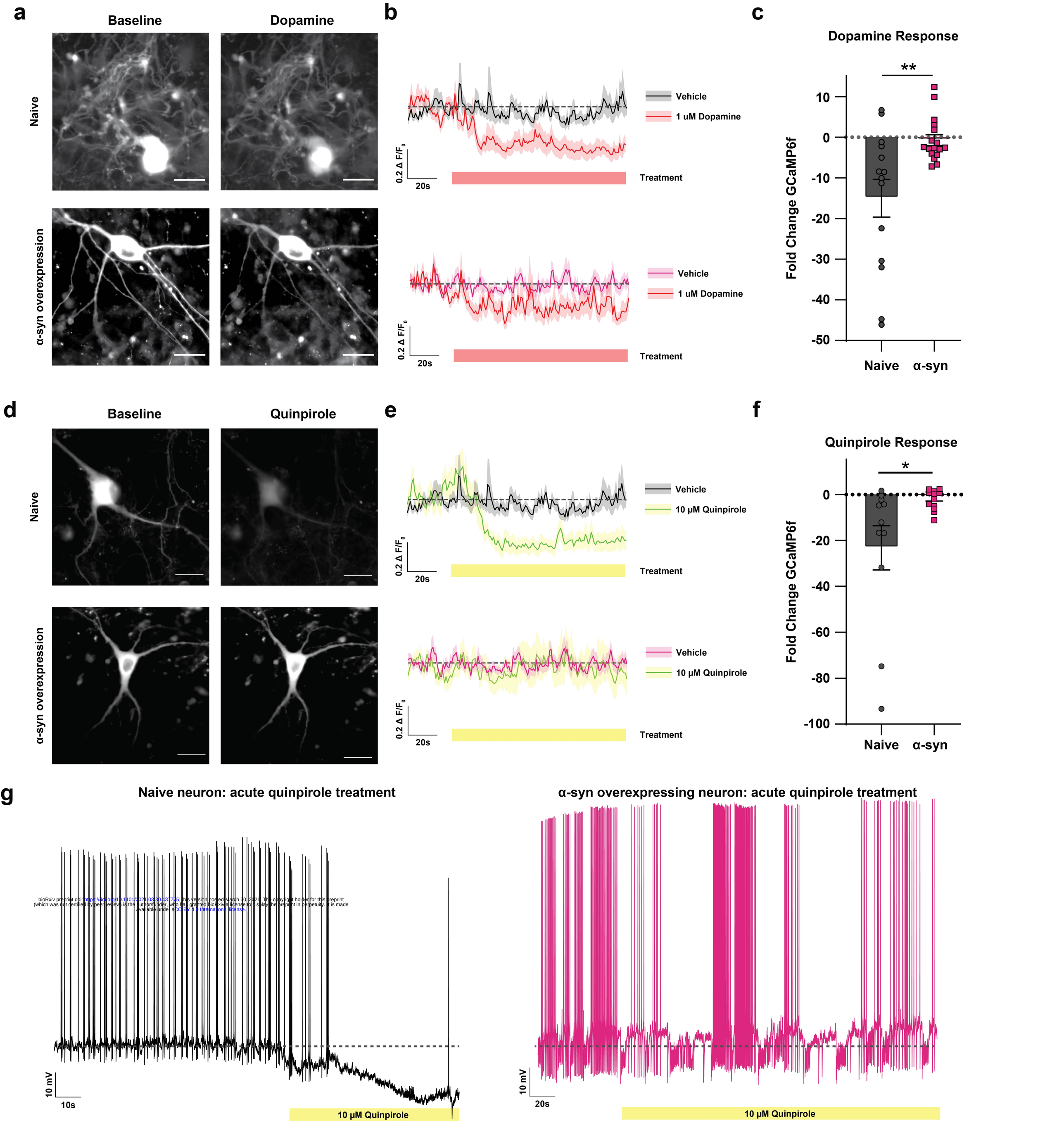

a

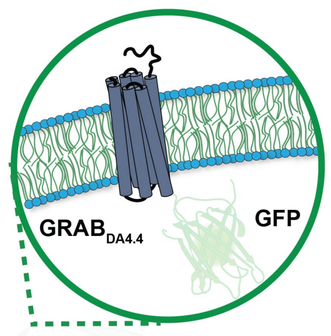

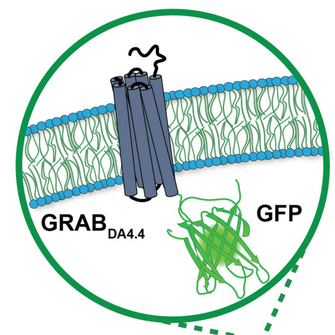

Increasing [DA] increases GRAB$_{DA4.4}$ fluorescence

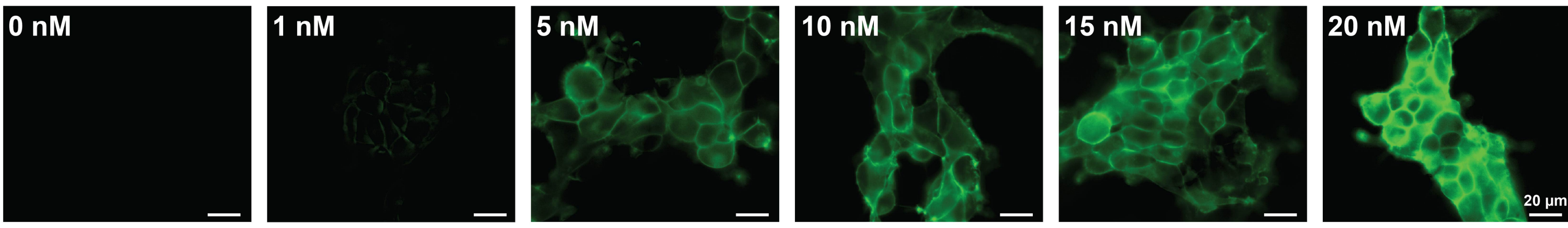

b

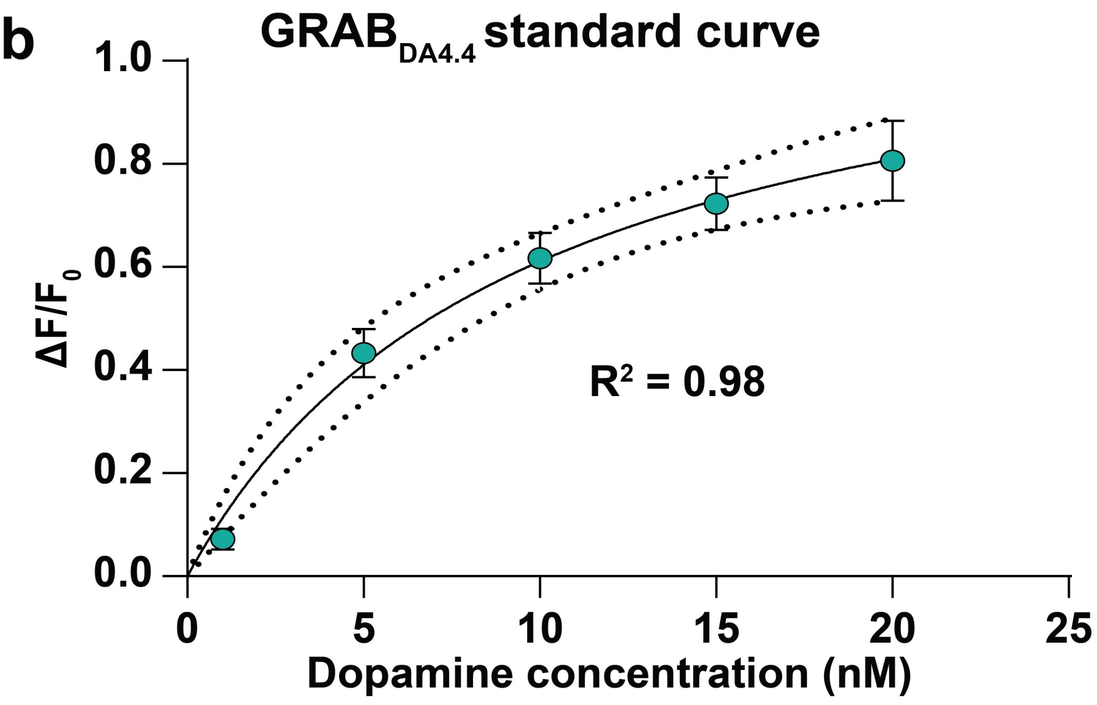

c

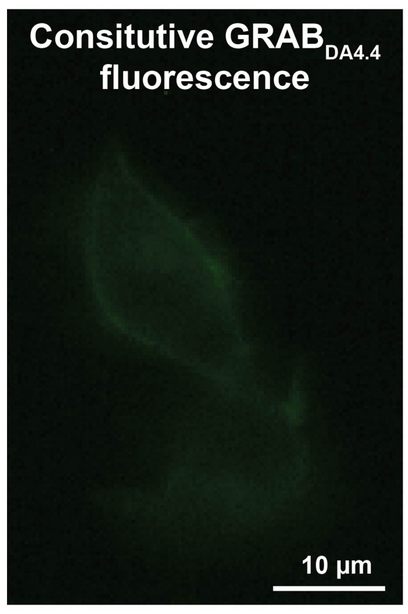

e

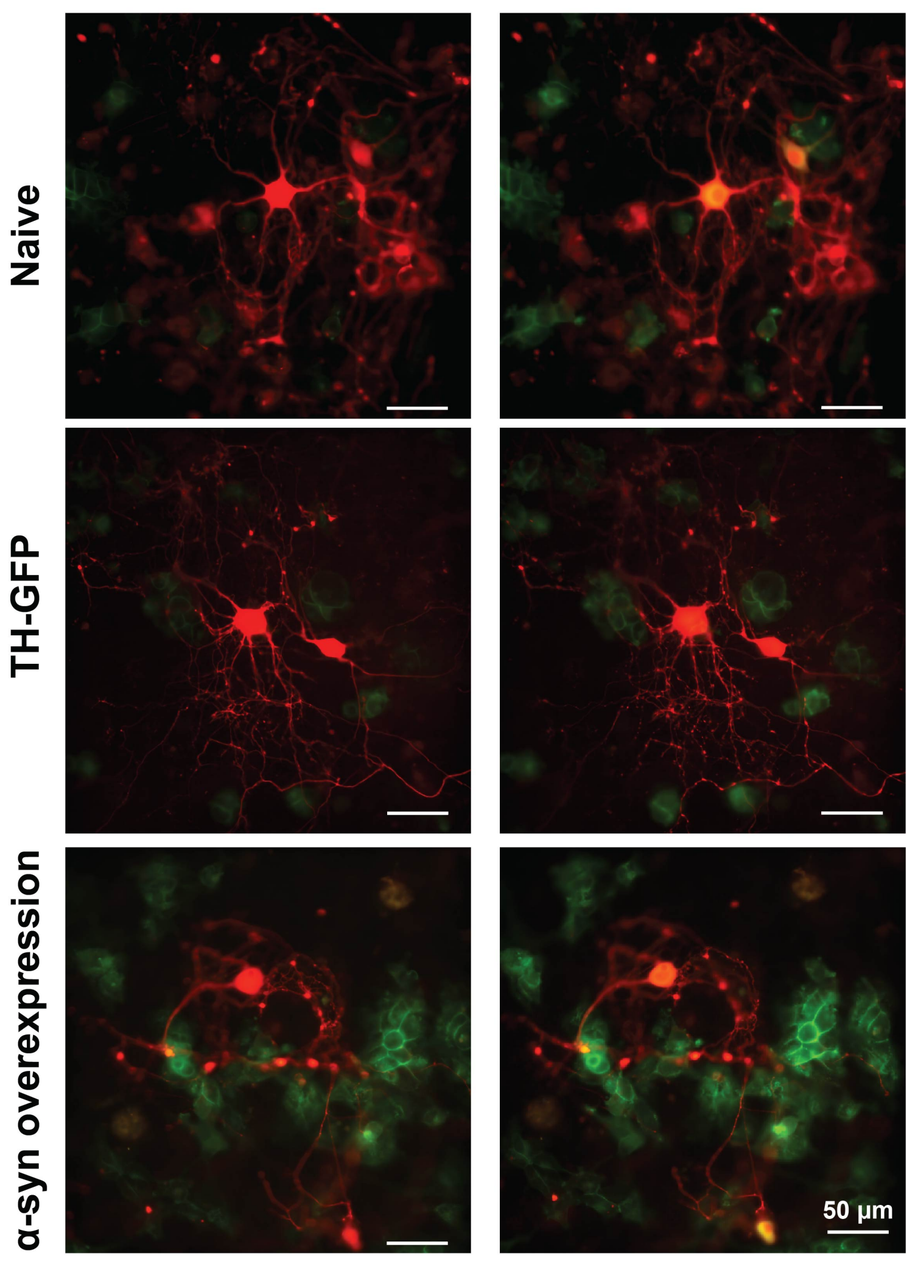

d

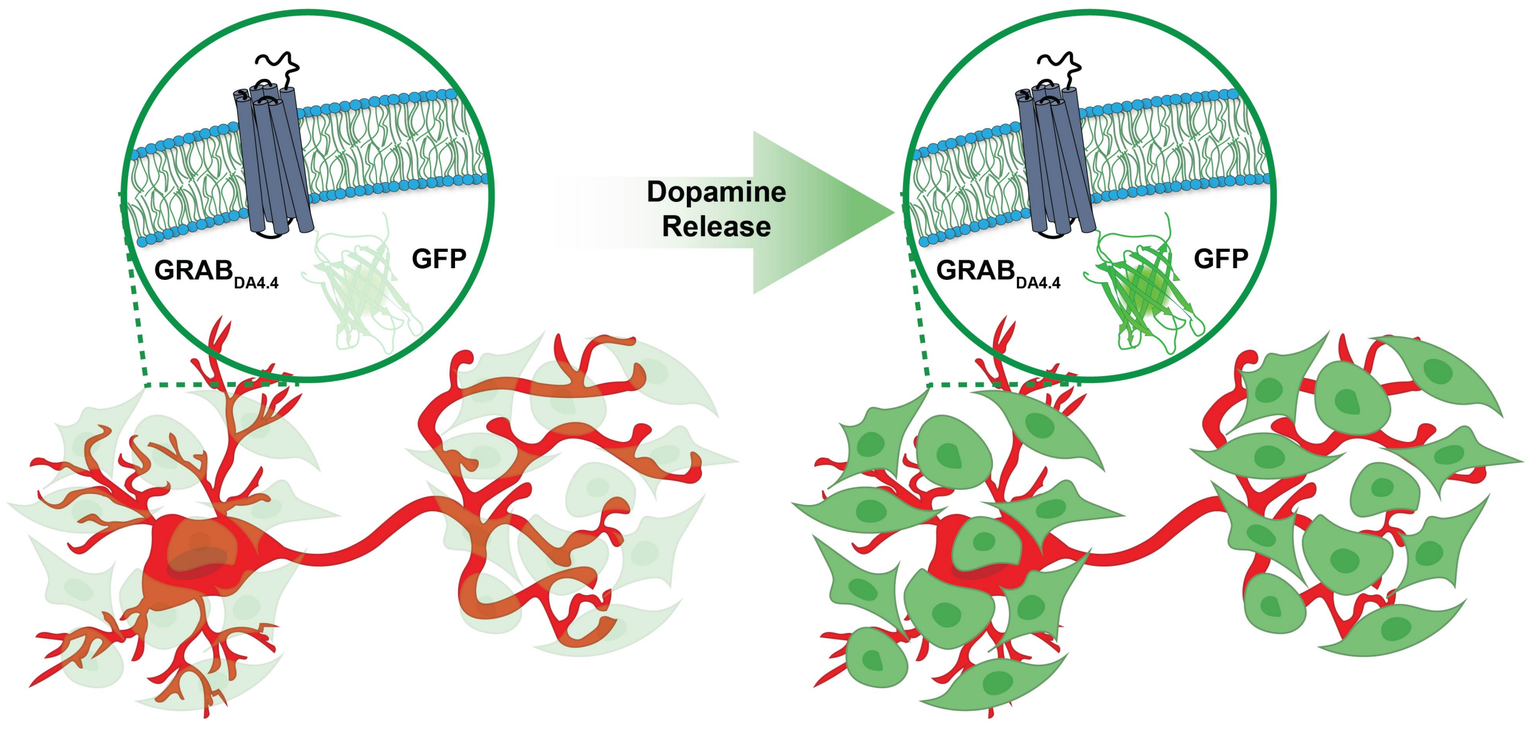

f

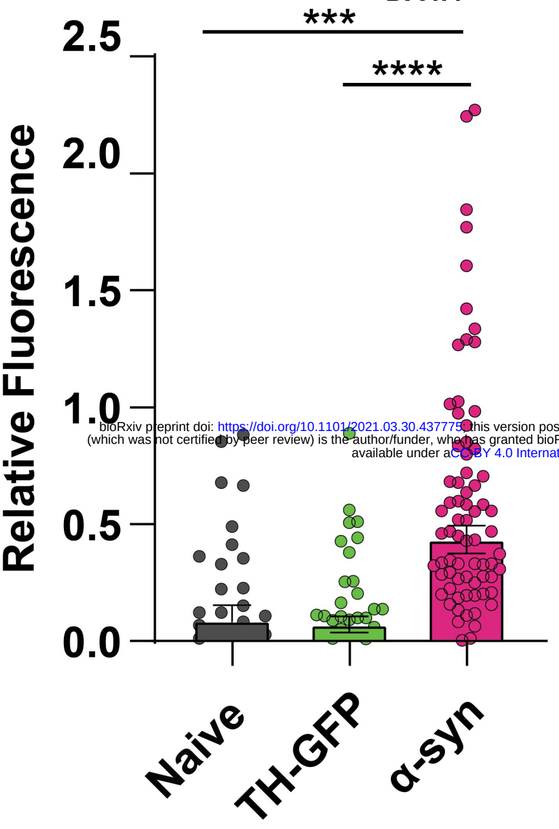

g

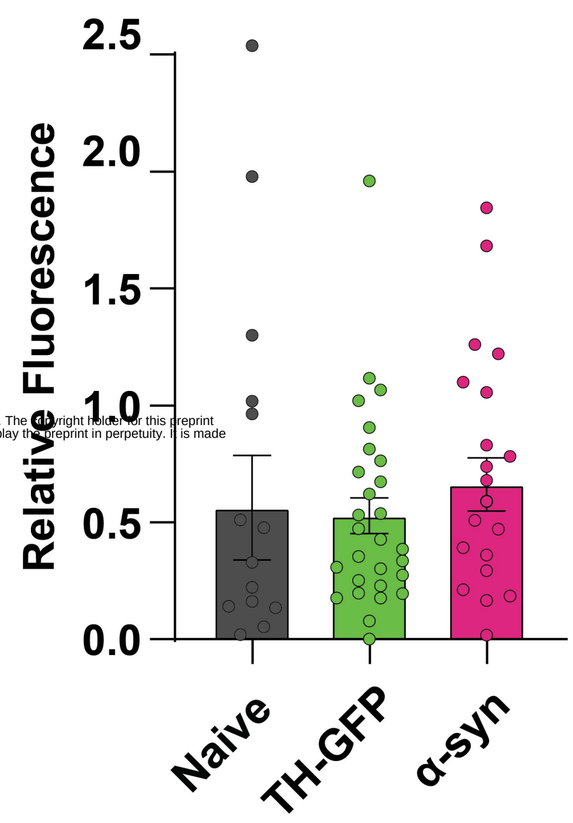

h

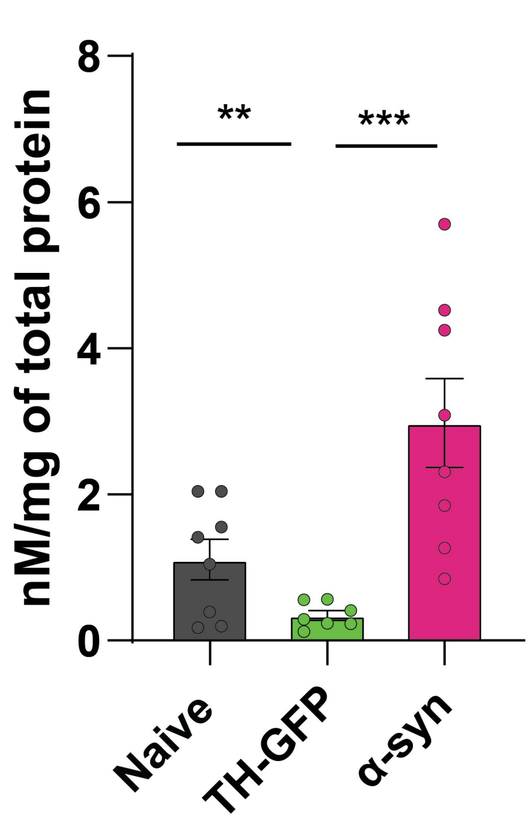

i

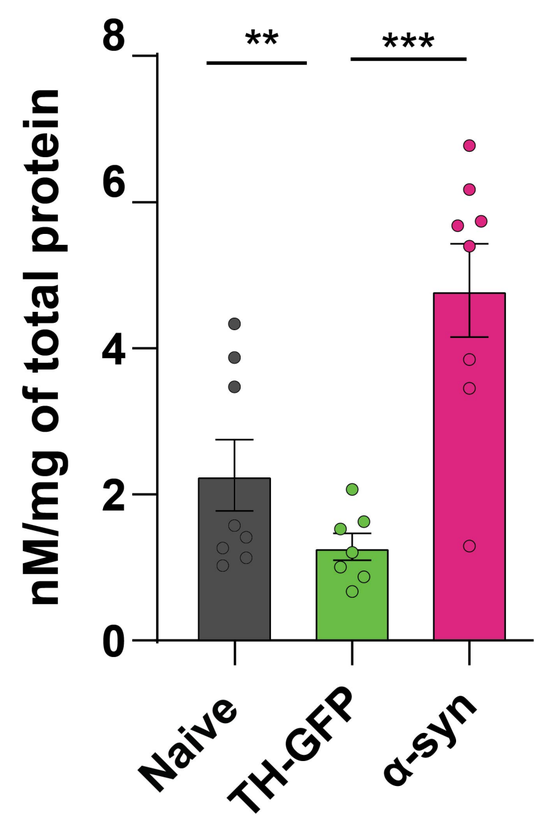

j

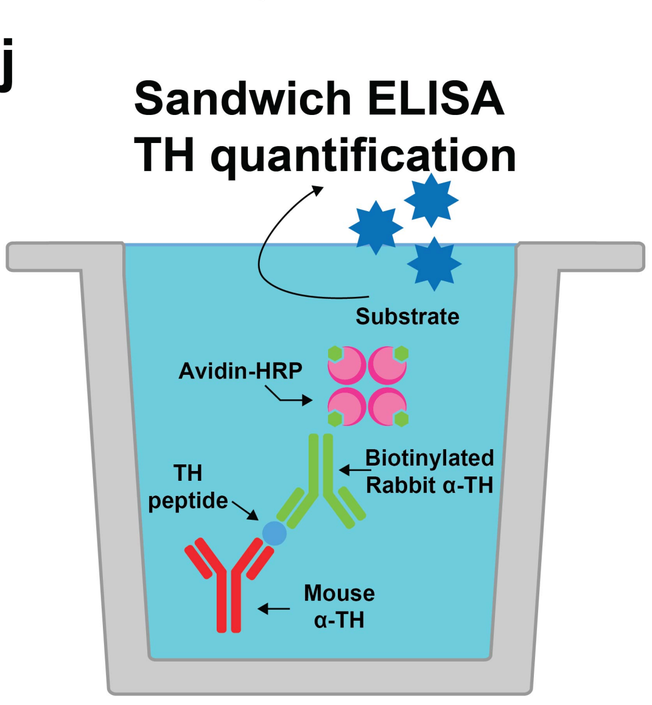

k

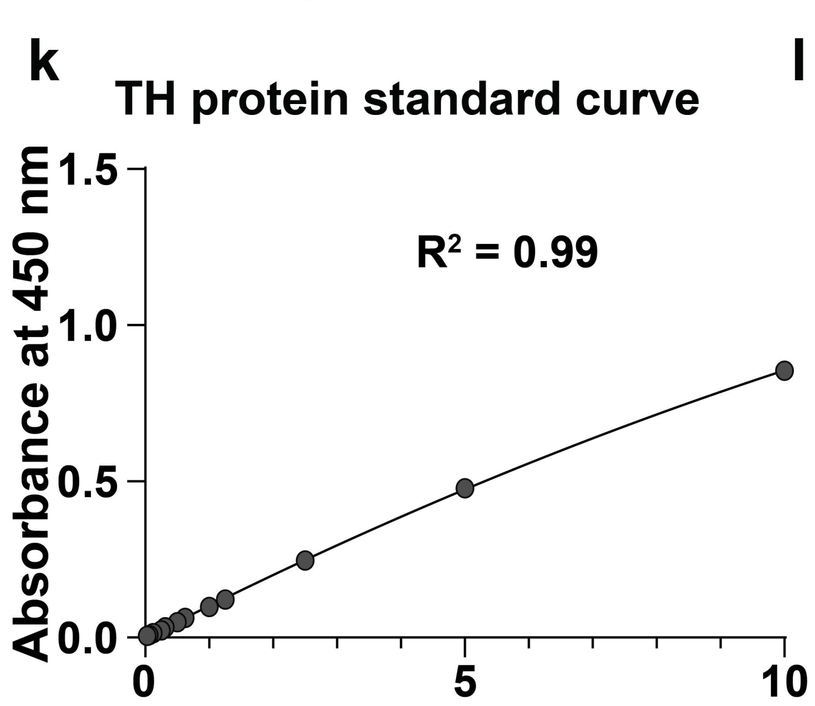

l

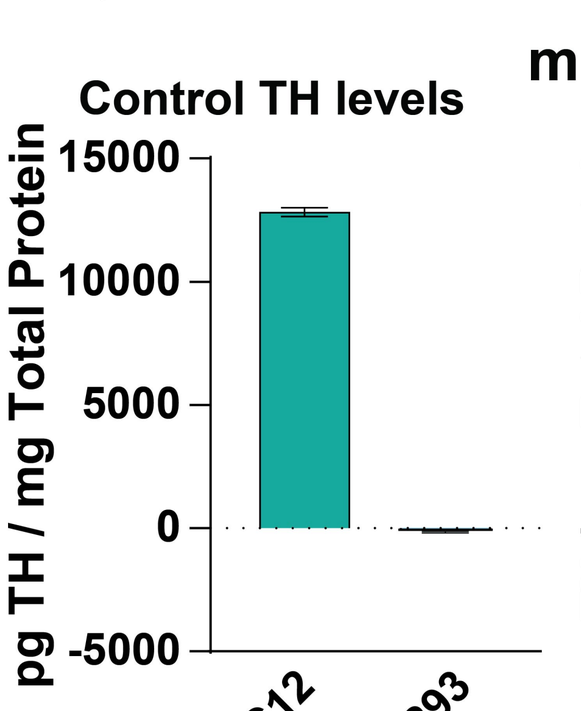

m

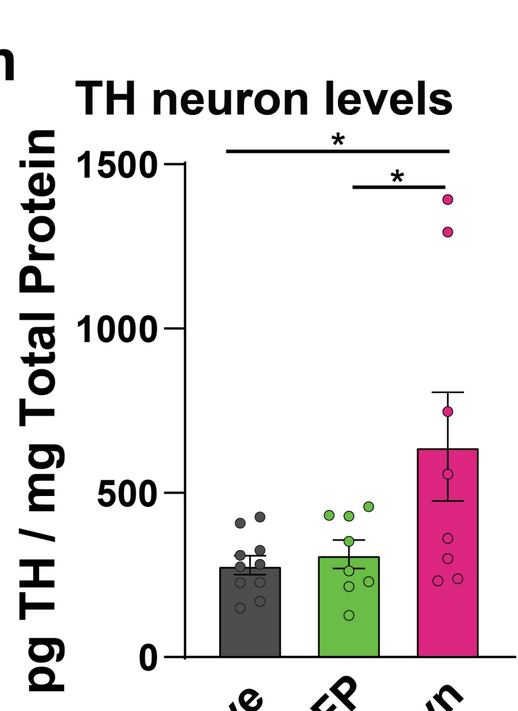

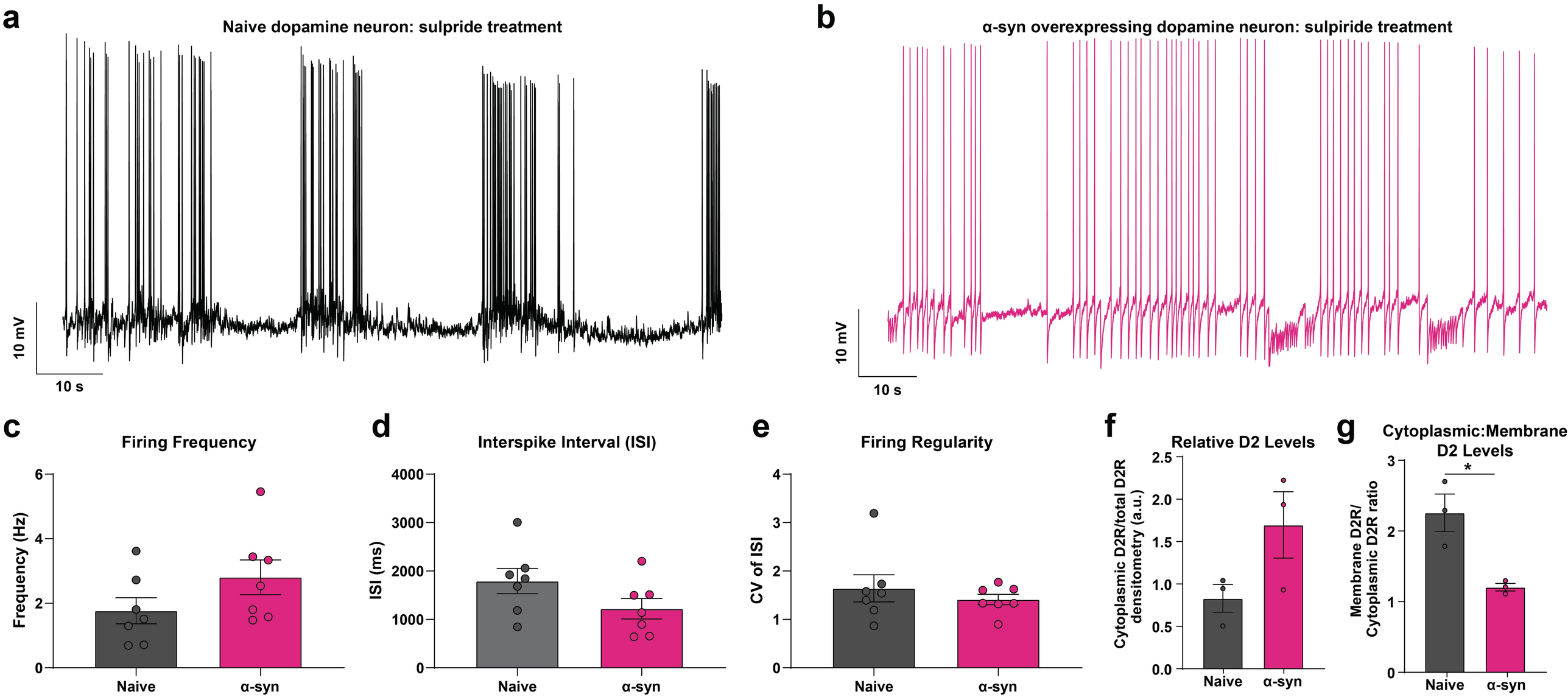
a
Naive dopamine neuron: sulpride treatment
10 mV
10 s
b
α-syn overexpressing dopamine neuron: sulpiride treatment
10 mV
10 s
c
Firing Frequency
Frequency (Hz)
0
2
4
6
Naive
α-syn
d
Interspike Interval (ISI)
ISI (ms)
0
1000
2000
3000
4000
Naive
α-syn
e
Firing Regularity
CV of ISI
0
1
2
3
4
Naive
α-syn
f
Relative D2 Levels
Cytoplasmic D2R/total D2R densitometry (a.u.)
0.0
0.5
1.0
1.5
2.0
2.5
Naive
α-syn
g
Cytoplasmic:Membrane D2 Levels
Membrane D2R/ Cytoplasmic D2R ratio
0
1
2
3
*
Naive
α-syn

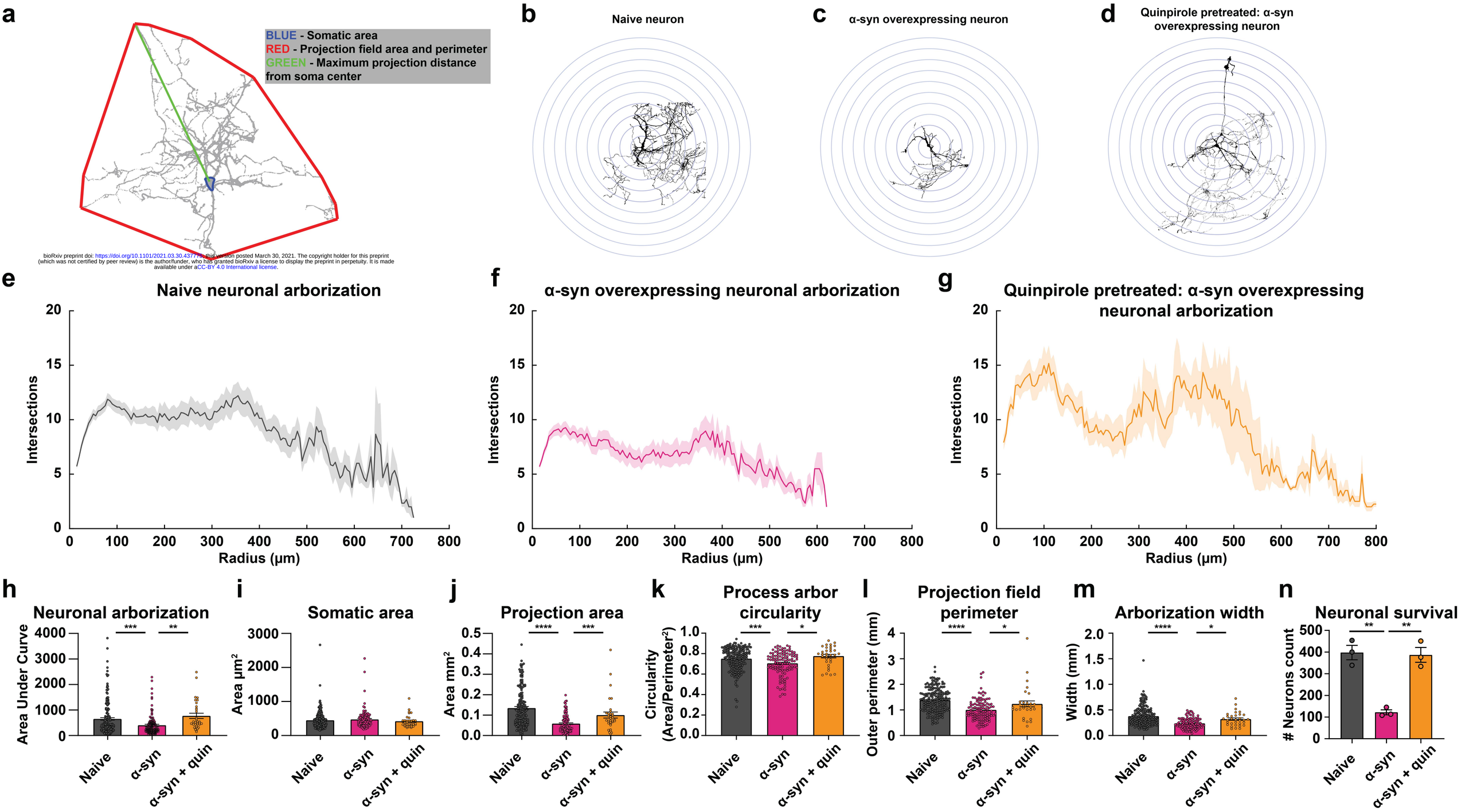

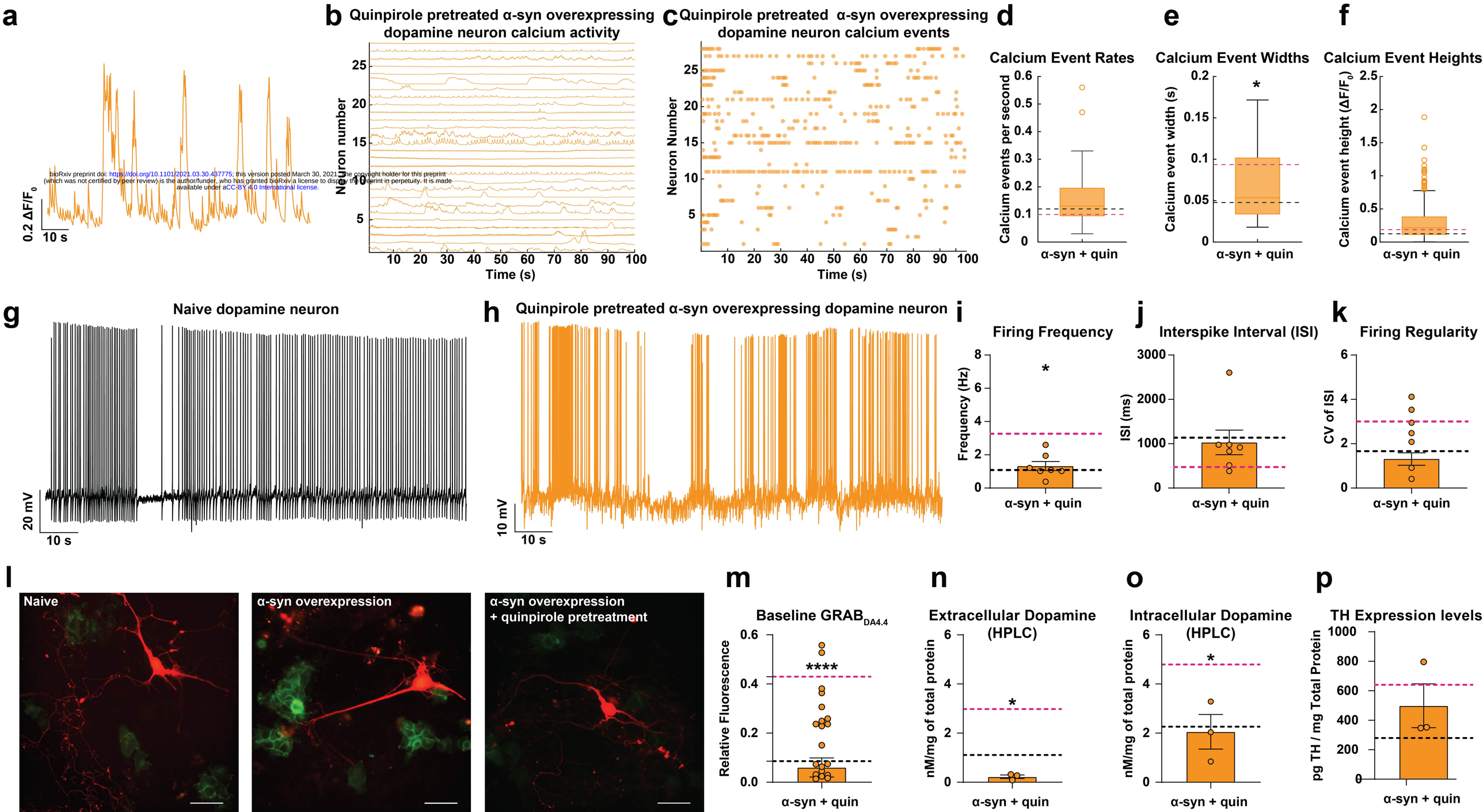

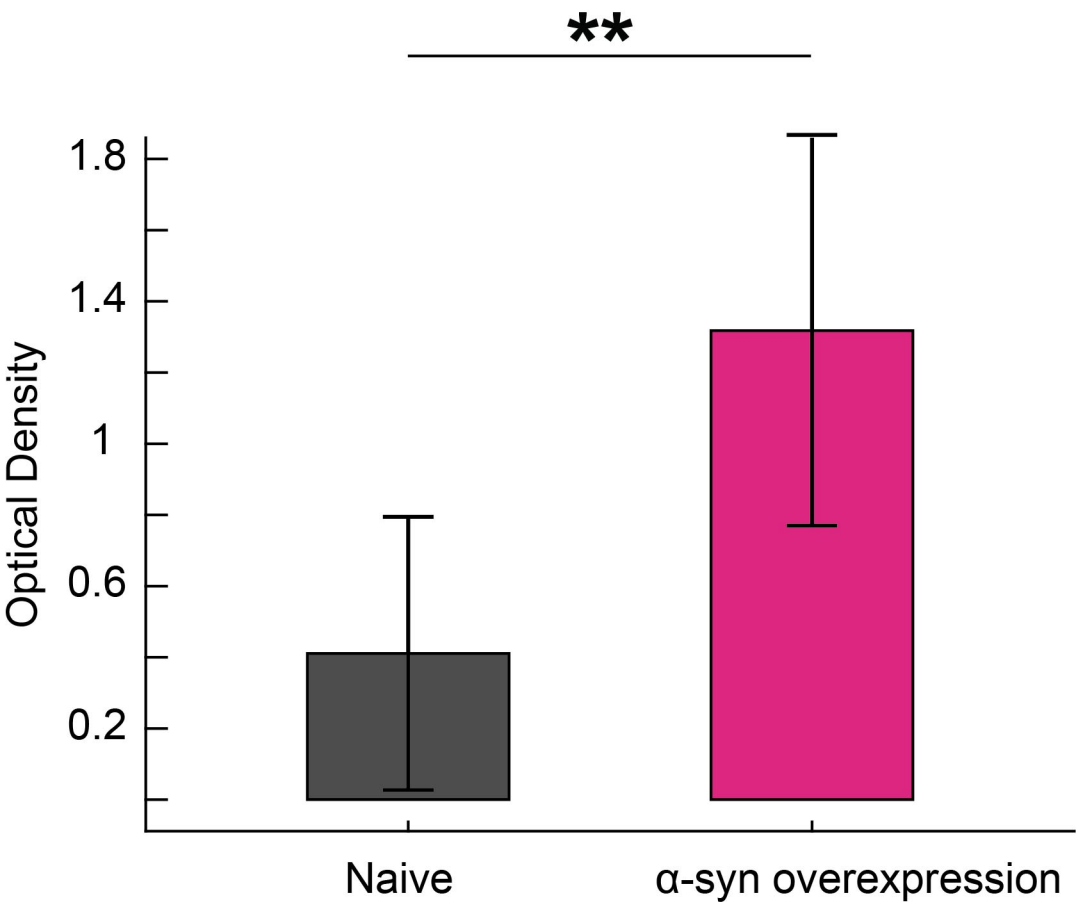
**
1.8
1.4
1
0.6
0.2
Optical Density
Naive
α-syn overexpression

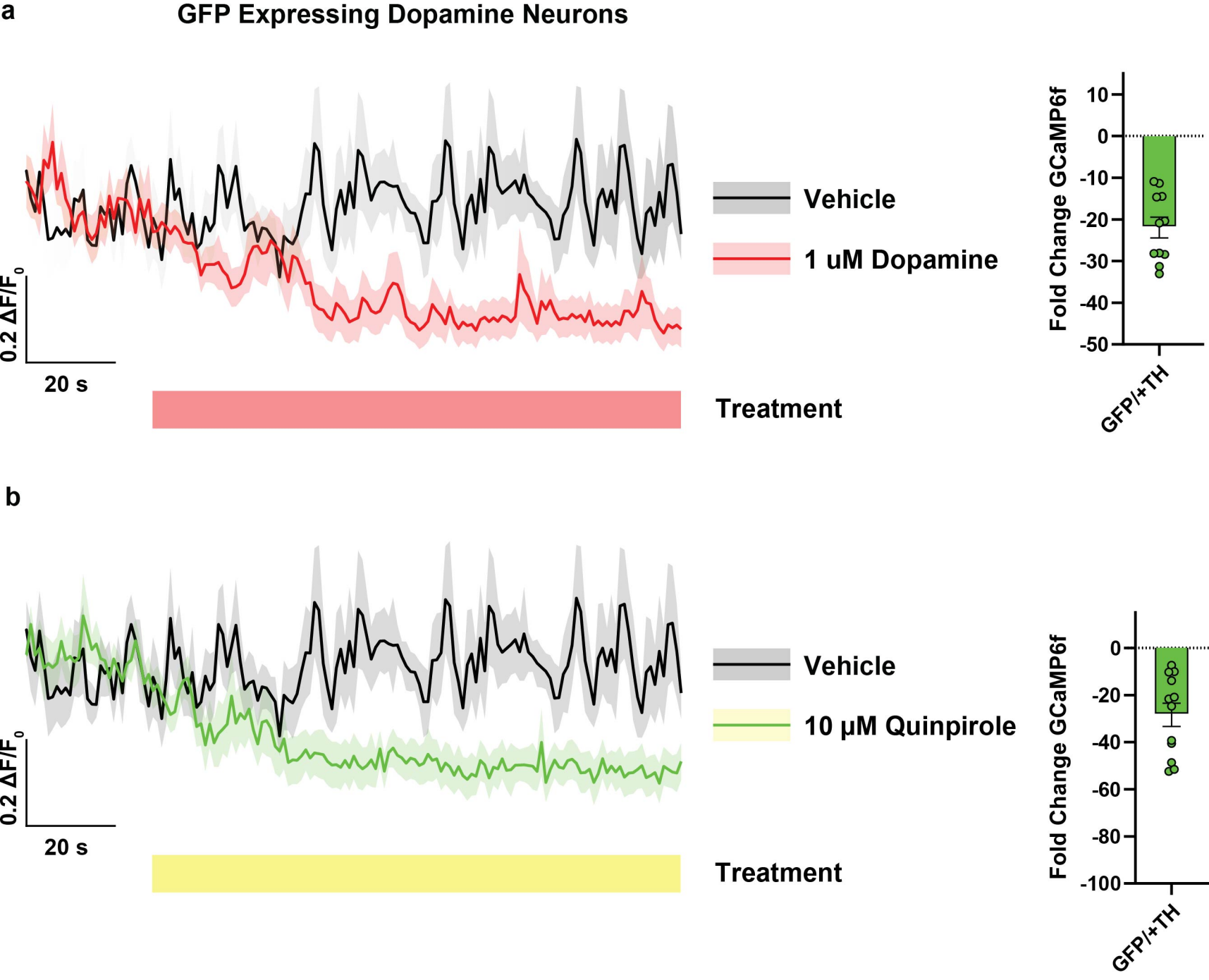
a
GFP Expressing Dopamine Neurons
0.2 ΔF/F0
20 s
Vehicle
1 uM Dopamine
Treatment
Fold Change GCaMP6f
10
0
-10
-20
-30
-40
-50
GFP/+TH
b
0.2 ΔF/F0
20 s
Vehicle
10 µM Quinpirole
Treatment
Fold Change GCaMP6f
0
-20
-40
-60
-80
-100
GFP/+TH